AFRL-ML-WP-TR-2004-4227

NONDESTRUCTIVE INSPECTION (NDI) FOR DIFFUSION BONDED COMPONENTS

Carl H. Smith, Ph.D.

NVE Corporation
11409 Valley View Road
Eden Prairie, MN 55344-3617

AUGUST 2003

Final Report for 09 May 2001 – 06 August 2003

This is a Small Business Innovation Research (SBIR) Phase II Report.

STINFO FINAL REPORT

MATERIALS AND MANUFACTURING DIRECTORATE
AIR FORCE RESEARCH LABORATORY
AIR FORCE MATERIEL COMMAND
WRIGHT-PATTERSON AIR FORCE BASE, OH 45433-7750

NOTICE

USING GOVERNMENT DRAWINGS, SPECIFICATIONS, OR OTHER DATA INCLUDED IN THIS DOCUMENT FOR ANY PURPOSE OTHER THAN GOVERNMENT PROCUREMENT DOES NOT IN ANY WAY OBLIGATE THE U.S. GOVERNMENT. THE FACT THAT THE GOVERNMENT FORMULATED OR SUPPLIED THE DRAWINGS, SPECIFICATIONS, OR OTHER DATA DOES NOT LICENSE THE HOLDER OR ANY OTHER PERSON OR CORPORATION; OR CONVEY ANY RIGHTS OR PERMISSION TO MANUFACTURE, USE, OR SELL ANY PATENTED INVENTION THAT MAY RELATE TO THEM.

THIS REPORT IS RELEASABLE TO THE NATIONAL TECHNICAL INFORMATION SERVICE (NTIS). AT NTIS, IT WILL BE AVAILABLE TO THE GENERAL PUBLIC, INCLUDING FOREIGN NATIONALS.

THIS TECHNICAL REPORT HAS BEEN REVIEWED AND IS APPROVED FOR PUBLICATION.

/s/

THOMAS J. MORAN, Project Engineer
Nondestructive Evaluation Branch
Metals, Ceramics & NDE Division

/s/

JAMES C. MALAS, Branch Chief
Nondestructive Evaluation Branch
Metals, Ceramics & NDE Division

/s/

GERALD J. PETRAK, Assistant Chief
Metals, Ceramics & NDE Division
Materials & Manufacturing Directorate

PUBLICATION OF THIS REPORT DOES NOT CONSTITUTE APPROVAL OR DISAPPROVAL OF THE IDEAS OR FINDINGS. IT IS PUBLISHED IN THE INTEREST OF SCIENTIFIC AND TECHNICAL INFORMATION EXCHANGE.

DO NOT RETURN COPIES OF THIS REPORT UNLESS CONTRACTUAL OBLIGATIONS OR NOTICE ON A SPECIFIC DOCUMENT REQUIRES ITS RETURN.

REPORT DOCUMENTATION PAGE

Form Approved
OMB No. 0704-0188

1. REPORT DATE *(DD-MM-YY)*	2. REPORT TYPE	3. DATES COVERED *(From - To)*
August 2003	Final	05/09/2001 – 08/06/2003

4. TITLE AND SUBTITLE
NONDESTRUCTIVE INSPECTION (NDI) FOR DIFFUSION BONDED COMPONENTS

5a. CONTRACT NUMBER
F33615-01-C-5207

5b. GRANT NUMBER

5c. PROGRAM ELEMENT NUMBER
65502F

6. AUTHOR(S)
Carl H. Smith, Ph.D.

5d. PROJECT NUMBER
3005

5e. TASK NUMBER
ML

5f. WORK UNIT NUMBER
AY

7. PERFORMING ORGANIZATION NAME(S) AND ADDRESS(ES)

NVE Corporation
11409 Valley View Road
Eden Prairie, MN 55344-3617

8. PERFORMING ORGANIZATION REPORT NUMBER

9. SPONSORING/MONITORING AGENCY NAME(S) AND ADDRESS(ES)
Materials and Manufacturing Directorate
Air Force Research Laboratory
Air Force Materiel Command
Wright-Patterson AFB, OH 45433-7750

10. SPONSORING/MONITORING AGENCY ACRONYM(S)
AFRL/MLLP

11. SPONSORING/MONITORING AGENCY REPORT NUMBER(S)
AFRL-ML-WP-TR-2004-4227

12. DISTRIBUTION/AVAILABILITY STATEMENT
Approved for public release; release is unlimited.

13. SUPPLEMENTARY NOTES
Report contains color. This is a Small Business Innovation Research (SBIR) Phase II Report.

14. ABSTRACT

This Phase II SBIR developed prototype eddy-current probe systems using Giant Magnetoresistance (GMR) and Spin Dependent Tunneling (SDT) sensors from the proof-of-concept probes developed in Phase I. These probes were designed for specific NDI problems. Samples were tested that emphasized the detection of multi-point failure in aircraft skins using an array of sensors to scan multiple rows of rivets and the detection of interlayer corrosion in multilayer aircraft skins. Laptop computer-based systems were developed using Labview software to display the results of surface scans. Both GMR and SDT sensors were incorporated in eddy-current probes including X-Y sensors with on-chip excitation coils, new shape-biased SDT sensors with reduced power consumption, and GMR sensor arrays with up to 16 elements.

15. SUBJECT TERMS
NDE, GMR Sensors, SDT Sensors, Eddy-current testing, GMR sensor arrays

16. SECURITY CLASSIFICATION OF:			17. LIMITATION OF ABSTRACT:	18. NUMBER OF PAGES	19a. NAME OF RESPONSIBLE PERSON (Monitor)
a. REPORT	b. ABSTRACT	c. THIS PAGE			Thomas J. Moran
Unclassified	Unclassified	Unclassified	SAR	64	19b. TELEPHONE NUMBER *(Include Area Code)* (937) 255-9800

Standard Form 298 (Rev. 8-98)
Prescribed by ANSI Std. Z39-18

TABLE OF CONTENTS

PAGES 1 - 2 WERE INTENTIONALLY LEFT BLANK

SUMMARY

The project was completed with most of its objectives met and in some cases expectations exceeded. The emphasis of the samples was changed from diffusion-bonded interfaces to detection of multi-point failure in aircraft skins using an array of sensors that can be used to scan multiple-rows of rivets and detection of interlayer corrosion in multilayer aircraft skins. Samples investigated included surface cracks, edge cracks, and deep edge cracks as well as samples simulating surface and interlayer corrosion.

Portable laptop computer based systems were developed using Labview software to display the results of surface scans by single-sensor probes and probes with arrays of sensors. Various GMR and SDT sensors were incorporated in eddy-current probes including X-Y sensors with on-chip coils, new shape-biased SDT sensors with reduced power consumption, and GMR sensor arrays with up to 16 elements. Integrated eddy-current probes with sensor arrays and instrumentation amplifiers were produced as well as systems with parallel processing of data from sensor arrays. Arrays to conform to specific geometries were not investigated, as the samples of interest were predominantly flat sheets.

During this program, Albany Instruments, Inc. tested specimens provided by the program monitor. The eddy current probes and methods previously developed under this project were used to detect the second-layer cracks around fasteners disposed in a row. Two cracks were detected in two of these specimens. The location of one crack was known – indicated by the program monitor.

Compilations were made of materials including ceramics and connectors for eddy-current probes and of eddy-current probe manufactures and their unique features,

Albany Instruments/University of North Carolina-Charlotte developed substantial intellectual property. A total of three disclosures have been written and a utility patent has been filed on one of them.

Efforts to commercialize the technology developed in this program included funded projects with companies both inside and outside the NDE community, e.g. SwRI. We also have quoted supporting other companies in NDE programs. Several papers presented the results from this program including papers at Aeromat2002, Quantitative NonDestructive Evaluation (QNDE), and Sensors EXPO.

PROGRAM OBJECTIVES

The objective of this Phase II project is to transfer the proof of concept eddy current probes which were developed during Phase I using GMR and SDT sensors into a family of prototype GMR/SDT based eddy current probe systems designed for specific NDI problems. Each design will be optimized for the detection and measurement of defects for specific industry requirements. Initially, five distinct probe designs will be investigated. These are:

1. Surface-crack detector –specialized probe for detection of small cracks initiating either at or far away from edges.
2. Deep edge-crack detectors – applied to multi-layer sandwich structures.
3. Integrated eddy current probe for small surface cracks.
4. Probe arrays for rapid data acquisition and patterned arrays to conform to specific specimen geometries.
5. Eddy current probe for evaluation of diffusion bonded interfaces.

DESCRIPTION OF WORK PERFORMED DURING THE CONTRACT EXTENSION PERIOD (May 7 – August 6, 2002)

The following work has been performed during this period:

1. A method for mapping buried cracks around fastener holes disposed in rows has been developed and tested. The probes previously developed were scanned over areas located at both sides of the fastener row (not above the symmetry axis) to detect buried transverse cracks.
2. The new 8-sensor GMR-array was provided by NVE and has been incorporated in the portable eddy current system developed by Albany. The system has been successfully tested in an experimental study on mapping edge cracks.

1. Two dimensional scans for mapping buried cracks around holes disposed in rows

Previous work demonstrated the capability of GMR eddy current probes to detect transverse cracks in a row of fastener holes. The method of detection used a single scan with the sensor over the symmetry axis of the holes line. Often a 2-D raster scan of a single sensor probe or a single scan of a linear array of sensors is preferred in order to obtain the map of the area scanned. Therefore an experimental study was conducted to determine the capability of the probe to map these defects when the probe was scanned off-axis, above areas located beside from the holes row.

In this experimental study, a specimen used in previous work was scanned – Figure 1. The plate has the thickness of 3.2 mm (0.125 in.), the width of approximately 50 mm (2 in.) and the length of 280 mm (11 in.). Ten holes of 6.3 mm (0.25 in.) diameter were drilled in each plate along the longitudinal symmetry axis of the plate. The distance between the centers of adjacent holes is 19 mm (0.75 in.). Two corner notches of 1 mm (0.04 in) in depth – less than one third of the plate thickness - were machined. The notches can be observed at hole #3 (left side) – the 2.5 mm long notch, and at hole #7 (right side) – the 2 mm notch. A probe comprising a flat coil having parallel wires and a GMR located above the center of the coil was manufactured. The flat coil is configured such that the currents in the central region flow in the same direction and have the return paths on the sides. The axis of sensitivity of the GMR sensor was oriented along the direction of the coil wires.

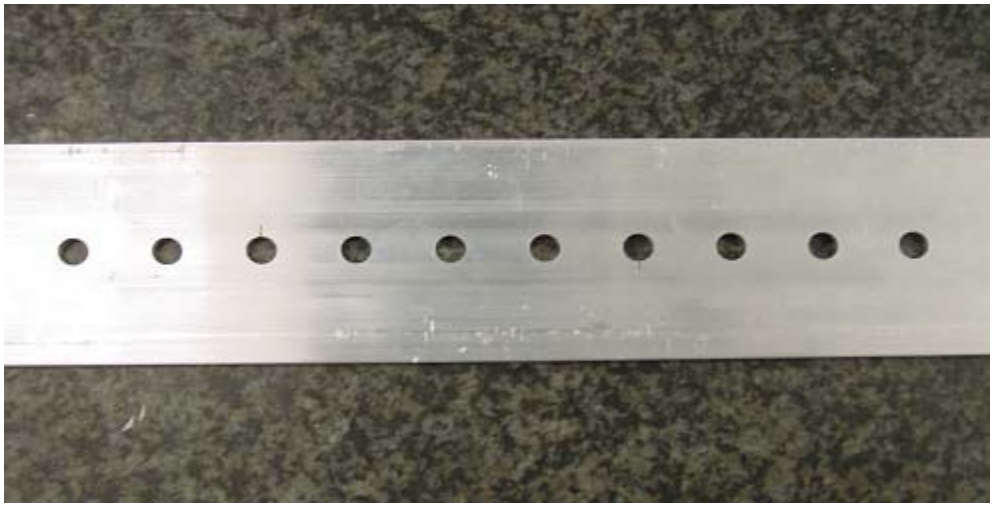

Figure 1. Plate containing a 2.5 mm left-side notch in hole #3 and a 2 mm right-side notch in hole #7. Holes are numbered 1 through 10 from left to right.

The probe was scanned above the specimen, with the defects at the bottom of the plate (buried at 3.2 mm under the surface). The configuration of the probe and specimen during scanning is shown in Figure 2. The probe was 2-D scanned such that the sensor passes over the light stripes indicated in Figure 2. These areas have a width of 4.5 mm and the middle of each stripe is located at 8 mm aside from the symmetry axis of the holes row. The positioning of the sensor outside the holes region was chosen to obtain maximum sensitivity to defects and minimum signals from the holes edges.

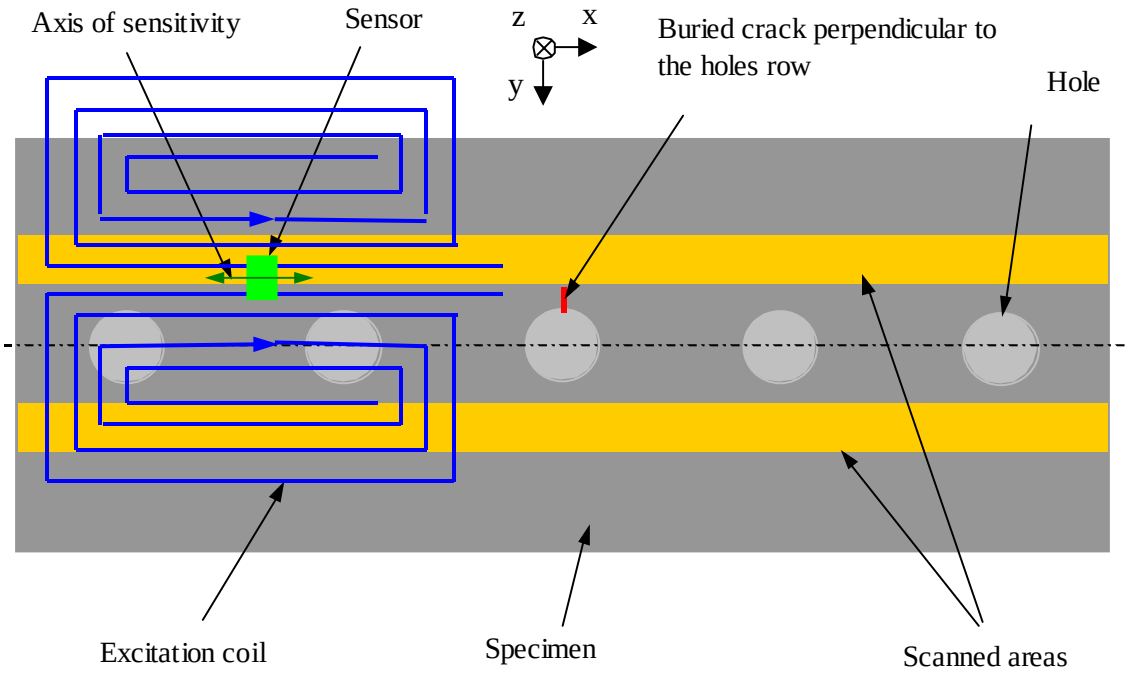

Figure 2. Detection of buried cracks around holes by scanning a GMR eddy current probe aside from the symmetry axis of the holes row.

An excitation frequency of 1 kHz was used for these scans. Figures 3 and 4 show the maps obtained from scanning the left side, respectively the right side of the specimen from hole #1 to hole #10 (the x- and y-axis on these maps are not scaled). The darker stripes on these maps correspond to the positions of the cracks (hole #3 - in Figure 3, and hole #4 – in Figure 4). It can be observed that the left crack in hole #3 is not visible on the map of Figure 4 corresponding to the right side, therefore the location of the defects can be accurately determined from these maps. Holes #1 and #10 also create darker images because they are positioned at the ends of the row.

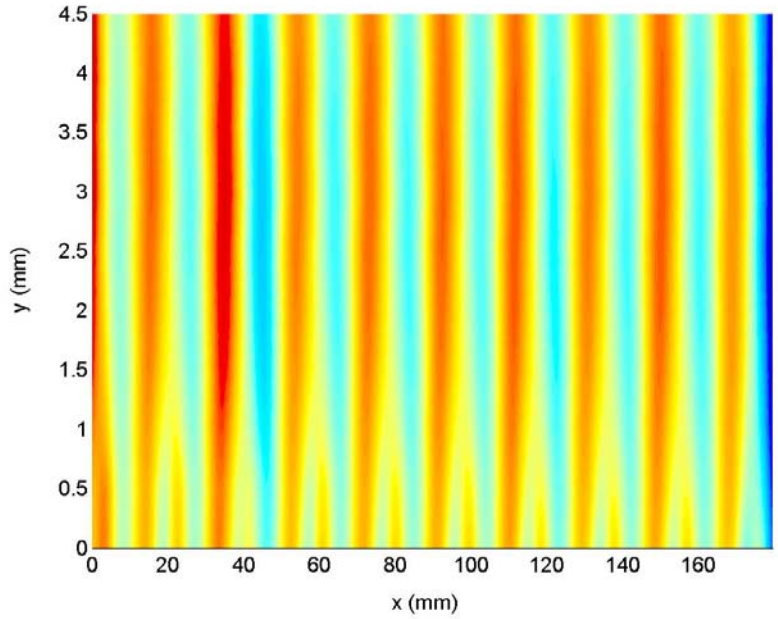

Figure 3. Map obtained from scanning an area located on the left side of the specimen shown in Figure 4. The dark stripe corresponds to the position of the left-side crack in hole #3 – buried at 3.2 mm under the surface.

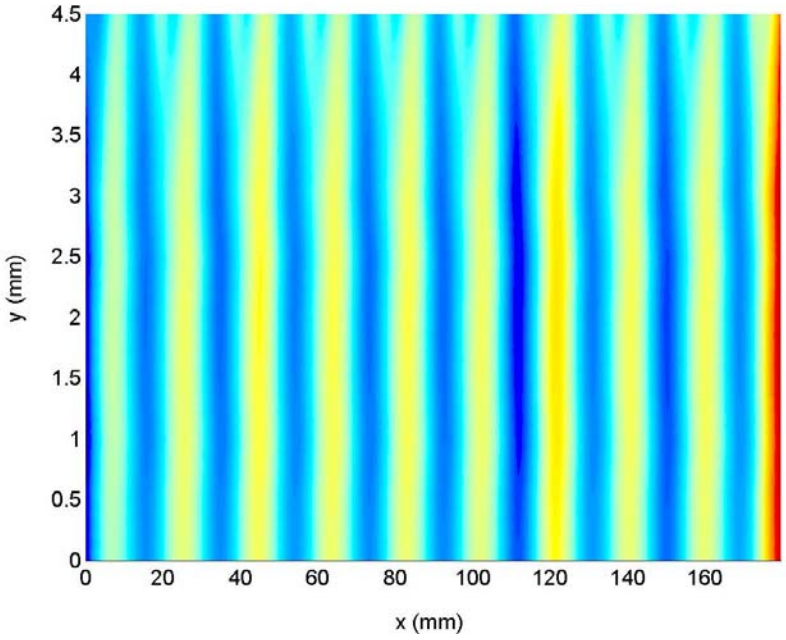

Figure 4. Map obtained from scanning an area located on the right side of the specimen shown in Figure 4. The dark stripe corresponds to the position of the left-side crack in hole #7 – buried at 3.2 mm under the surface.

This method offers several advantages as compared to the method of detection on the symmetry axis of the fastener holes row:

a. No precise alignment of the probe over the row axis is necessary.
b. If there are two transverse cracks in a hole symmetrically disposed about the symmetry axis of the row, the method based on symmetry is not capable to detect them.
a. The maps resulted from two dimensional scans contain more information about the location and size of defect than the plot resulted from a single scan along the symmetry axis.

2. Test of the GMR-array based eddy current system for mapping buried defects

An experimental study for mapping edge cracks has been conducted to test the newly developed GMR-array based eddy current system developed at Albany. In a previous report the system featuring a very dense GMR array has been used for mapping the magnetic field created by a small solenoid.

A new array of eight (8) GMR sensors spaced at 0.5 mm pitch has been provided by NVE. The sensors in the array are high-temperature multi-layer AAH002 full bridge sensors having 16:1 flux concentrators. The total width of the array is 3.5 mm. Unlike the array used in the previous study, the new array cannot be directly connected to the data acquisition card of the computer. A board comprising eight identical instrumentation amplifiers and high-pass filters has been built for the interface between the sensor array outputs and the DAQ card. In this way, the output signal of each sensor was amplified by a factor of 10 and the DC component was eliminated.

The signals are processed in parallel by using the software simulated lock-in amplifiers developed by Albany. Although this experimental study uses only eight sensor array inputs of the DAQ card, up to 16 sensor signals can be simultaneously processed using this system. Because the sensors in the array were not matched in terms of sensitivity, the array was calibrated in a uniform AC magnetic field. Each sensor output was monitored. Sensitivity variation of about 15% between sensors was found. Based on the results recorded, correction factors were introduced in the software program that processes the signals from the array.

The specimen used in this experimental study was an aluminum plate of 11 mm in thickness, 154 mm in length and 76 mm in width. Two corner slots were machine at the middle of the two opposite edges of the plate - see Figure 5. Both slots have the depth of 3 mm. The first slot has the length of 15 mm, while the second one has the length of 3 mm.

A probe comprising a D-shaped coil of 45 mm radius and the GMR array of sensors placed on its axis of symmetry, external to the coil, was scanned along the two edges to map the notches. The sensitive axes of the sensors in the array are oriented along the straight side of the D coil, and along the edges scanned, as shown in Figure 5.

.

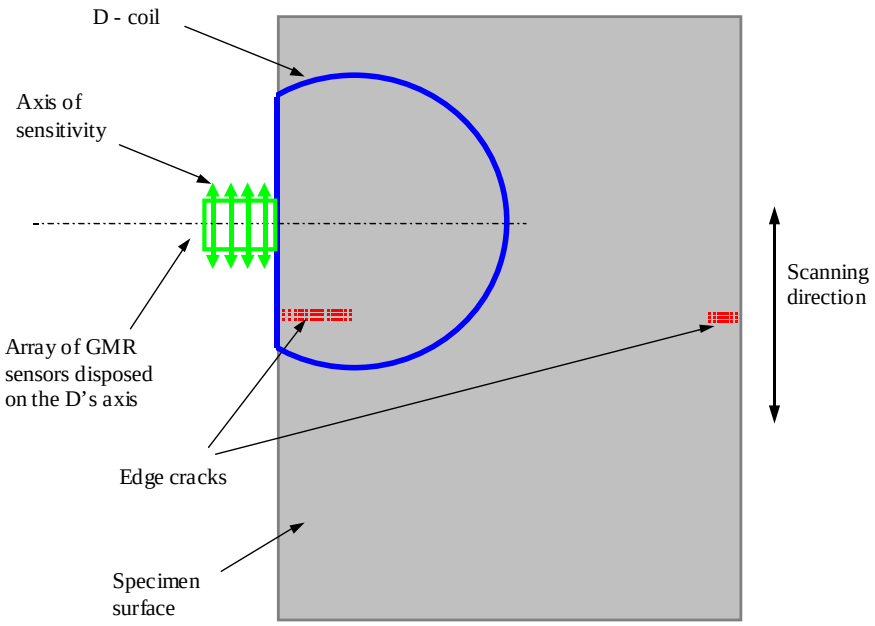

Figure 5: Schematic diagram showing the probe-specimen configuration for mapping edge cracks using an array-based eddy current probe.

The probe was linearly scanned along the edges containing the cracks, with the linear side of the coil above the edge. In this way high-density eddy currents are concentrated at the edge. Four scans were performed, such that each slot was mapped as either a surface defect or as a defect buried at 11 mm under the surface (when the specimen was flipped on the other side).

The maps obtained were the results of only one linear scan by monitoring the output of the eight sensors of the array simultaneously. The following scanning parameters were used in these experiments: scanning speed – 1 mm/s; number of data points along the scanning direction – 70; spacing of data points in y-direction - 1 mm; spacing of data points in x-direction - 0.5 mm (the pitch of the array). All four scans were performed with an excitation frequency of 200 Hz. A current of 1 A was passed through the D-coil. The in-phase (X) component was recorded for mapping the surface defects, while the out-of-phase (Y) component was monitored for mapping the buried defects.

The maps of the long defect (15 mm in length) are shown in Figures 6 – for the buried defect, and Figure 7 – for the surface defect. The amplitude of the signature for the buried defect was 5 mV, while the amplitude of the same defect at the surface was 12 mV. It is interesting to note that the distance between the two peaks (or the distance between the two dark stripes) is significantly different in these two maps. The peaks distance is about 14 mm for the buried crack, and 8 mm for the surface crack. Also the gradient in x-direction of the field is more visible in Figure 7 (for surface crack). The lateral spreading of the field created by deeply buried cracks is much greater than in the case of surface cracks, even the same frequency is used. The distance on z-axis between the probe and the defect contributes to this effect.

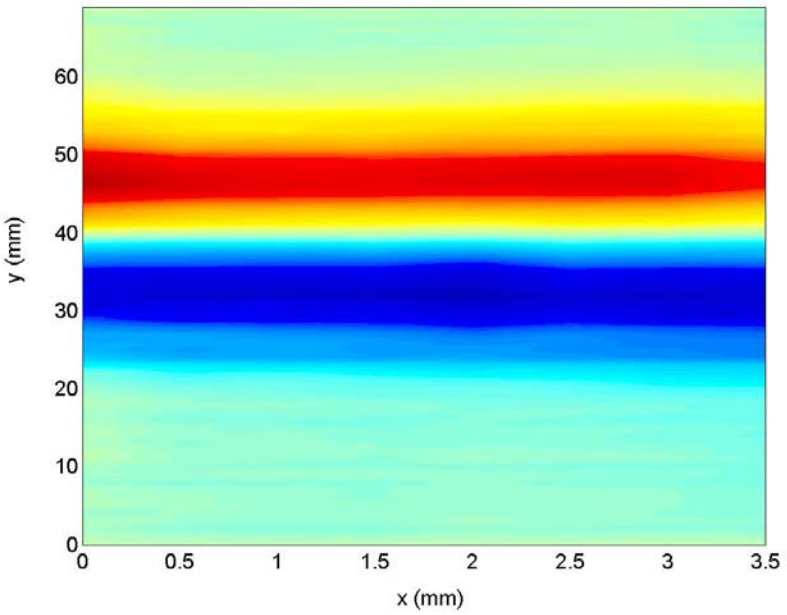

Figure 6: Map of the 15 mm long crack buried at 11 mm under the surface

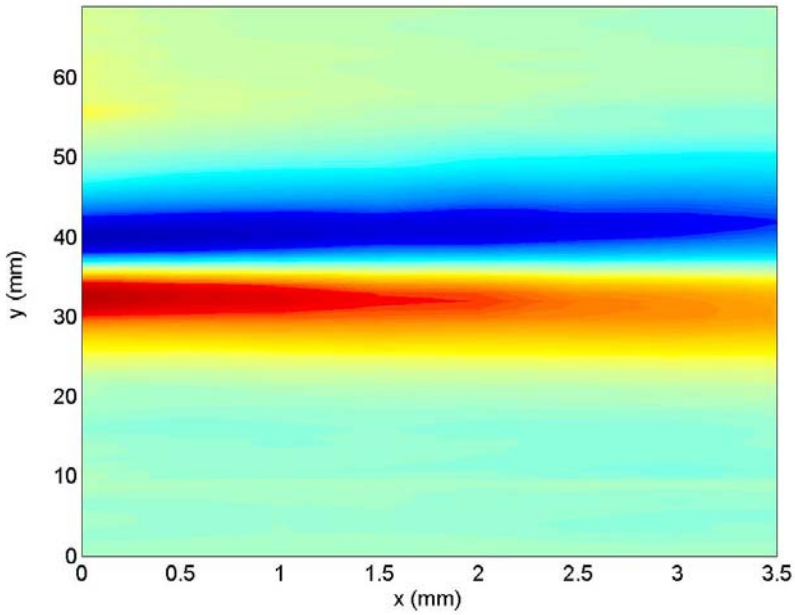

Figure 7. Map of the 15 mm long crack located at the surface of the specimen.

This effect is more visible when mapping the short edge crack of 3 mm length. Figures 8 and 9 show the maps for this defect when buried, respectively when at the surface. The amplitude of the signature for the short buried defect was 1.8 mV, while the amplitude of the same defect at the surface was 3 mV.

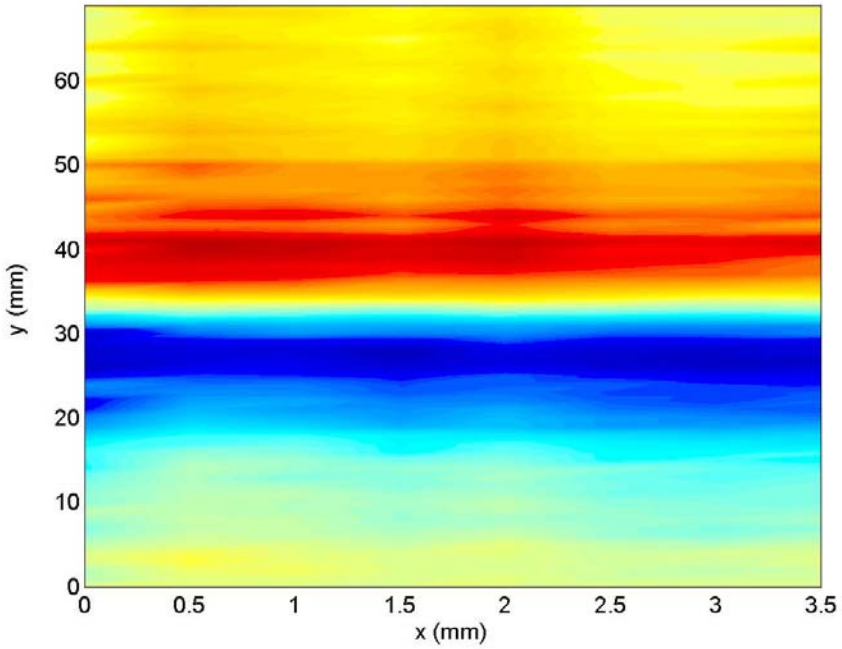

Figure 8. Map of the 3 mm long crack buried at 11 mm under the surface.

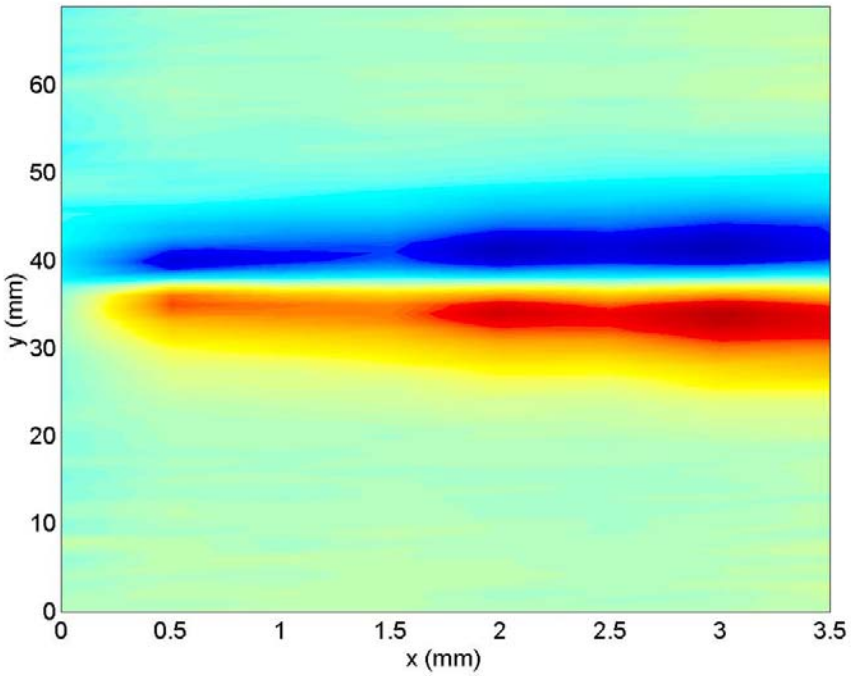

Figure 9. Map of the 3 mm long crack located at the surface of the specimen.

This study leads to an important conclusion regarding the pitch of the sensor arrays used for mapping buried defects. The spacing of the sensors in the array depends on the depth of the defects. For deeply buried flaws a greater spacing of the sensors is necessary to detect the field gradients created by a defect. In our example we consider that an array of eight sensors spaced at about 2 mm (covering 16 mm in width) would be more suitable to map defects located at about 10 mm under the surface.

This study demonstrated the capability of the newly developed GMR-array based eddy current system to map deeply buried flaws such as corner cracks. This system can be also used for mapping cracks around holes.

SUMMARY OF PHASE I PROJECT

During the phase I project, several different types of eddy current probes were designed and optimized for specific types of defects encountered in practice. In particular, three types of defects (cracks) were addressed:

1. Short surface cracks
2. Short surface edge cracks
3. Deeply buried edge cracks

A comparative study on the use of giant magnetoresistive (GMR) sensors and spin-dependent tunneling (SDT) sensors as detecting elements within the probe was undertaken.

The influence of the relative orientation of the sensitive axis of the GMR sensors with respect to the crack direction was assessed. A two-directional GMR sensor of orthogonal axis was designed and manufactured.

The first integrated eddy current probe containing a two-directional GMR sensor and an excitation coil deposited on the same substrate for high-resolution detection of short cracks was designed. The integrated eddy current probe on silicon chip opens the perspective for manufacturing of low cost integrated arrays of such probes. These arrays can be embedded in the structures inspected for in-situ monitoring of fatigue cracks.

A GMR sensor was successfully used for imaging a copper penny demonstrating the ability to detect surface features less than 1 mm high with less than 1 mm resolution.

An SDT sensor was successfully used for detecting deeply buried edge cracks at 15 mm below the surface.

The main technical goal of this project, that of assessing a compact, high-sensitivity eddy-current device with increased spatial resolution was accomplished. NVE was able to furnish UNC-C with SDT sensors of increasing

sensitivity even though the SDT sensors designed in this project were not yet finished. Compact eddy current probes with high sensitivity and high spatial resolution were demonstrated although ASIC chips were not integrated into the sensors. Detection of various types of flaws was demonstrated. Diffusion bonded components were not obtained for test.

SUMMARY OF RESULTS FROM PHASE II PROJECT

1. Sensor Development

At the beginning of the Phase I program, several wafers with sensors started in Phase I were packaged in 8-pin SIOC packages. These wafers had X-Y GMR sensors with1:1 and 3:1 flux concentrators, some with on-chip excitation coils. Figure 10 shows the diagram of a two-axis X-Y sensor with 3:1 flux concentrators. It consists of two completely independent Wheatstone bridge sensors with two active GMR elements and two shielded GMR elements acting as references. The size of the die is 2 mm by 2 mm. Each sensor is sensitive only to the component of magnetic field along its sensitive direction.

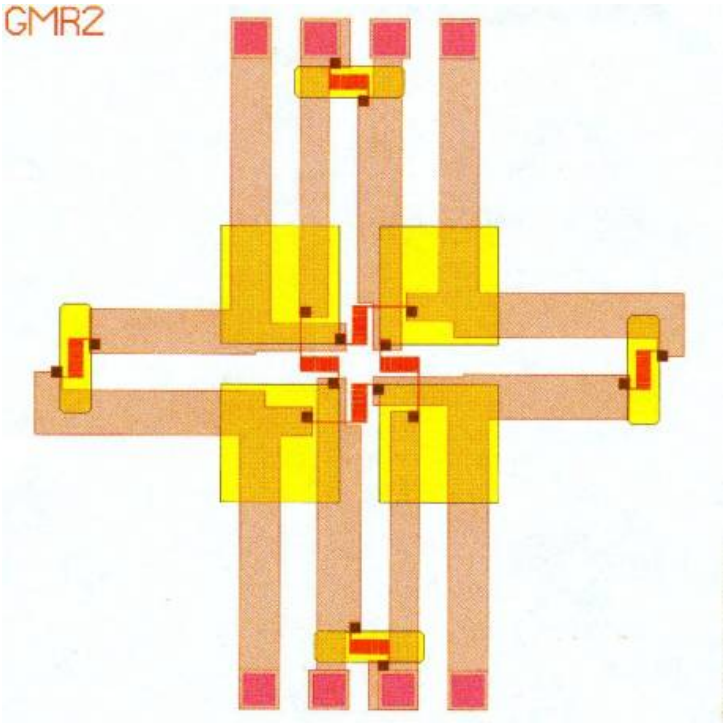

Figure 10. Diagram of a two-axis X-Y sensor consisting of two independent Wheatstone bridges.

A second type of sensor used in this project was a 16-element array of half bridges. Figure 11 shows a diagram of such an array with 15 μm spacing on a 1 mm by 2 mm die. Most of the space on the die is taken up by the bonding pads on the edge of the die. Lap-line monitors are located on either end of the array so that the edge of the die can be lapped to the edge of the sensing elements in order to minimize the stand off between the array and the sample. Figure 12 shows a diagram of four individual elements of the array with parts of several metal layers removed to make the structure clear.

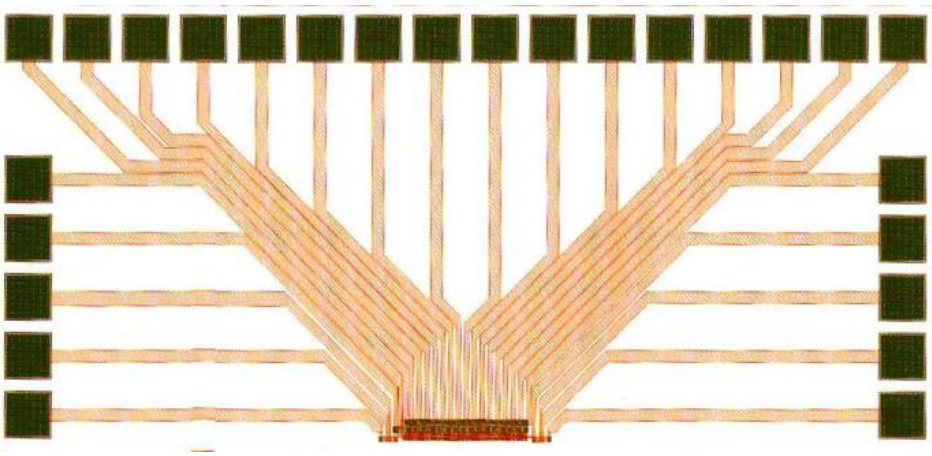

Figure 11. Diagram of a GMR sensor array with 16 half-bridge elements with 15 μm spacing at the bottom of a 1 mm by 2 mm die.

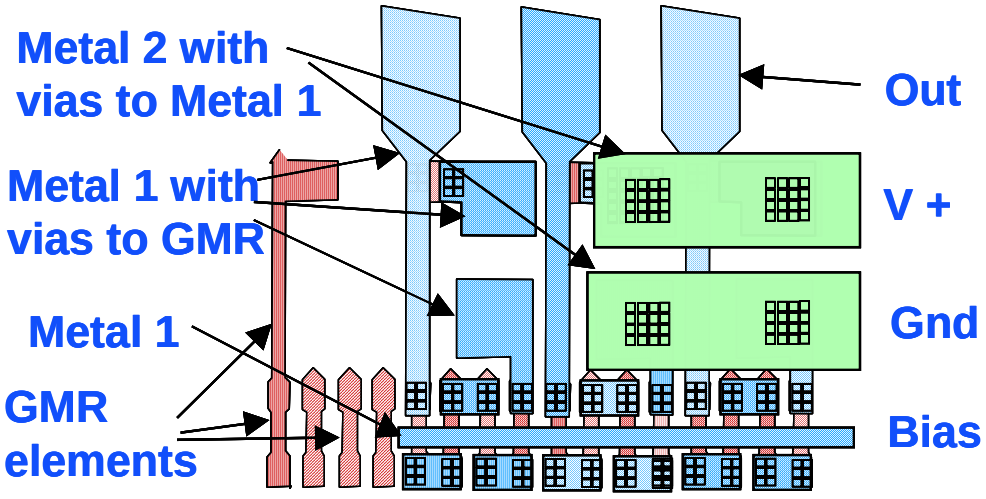

Figure 12. . Four individual elements of a 16-element array of GMR half-bridge sensors with 15 μm spacing. For clarity, the first elements are shown without metal 1 and metal 2 layers and without metal 1 layers.

The materials used in these sensors were chosen from three available GMR materials made at NVE. Magnetoresistive materials exhibit a change in resistance with magnetic field. Figure 13 shows the MR response (resistance as a function of magnetic field) of these multilayer materials.

The slopes of the GMR curves in Fig. 13 are 0.04 %/G for a conventional multilayer (ML), 0.07 %/G for a low-hysteresis multilayer (LH-ML), and 0.2 %/G for a high sensitivity multilayer (OD-ML) material. In a half bridge sensor configuration, these values correspond to outputs of 0.2, 0.35, and 1.0 mV/V/G (20, 25, and 100 nV/nT @ 10 V).

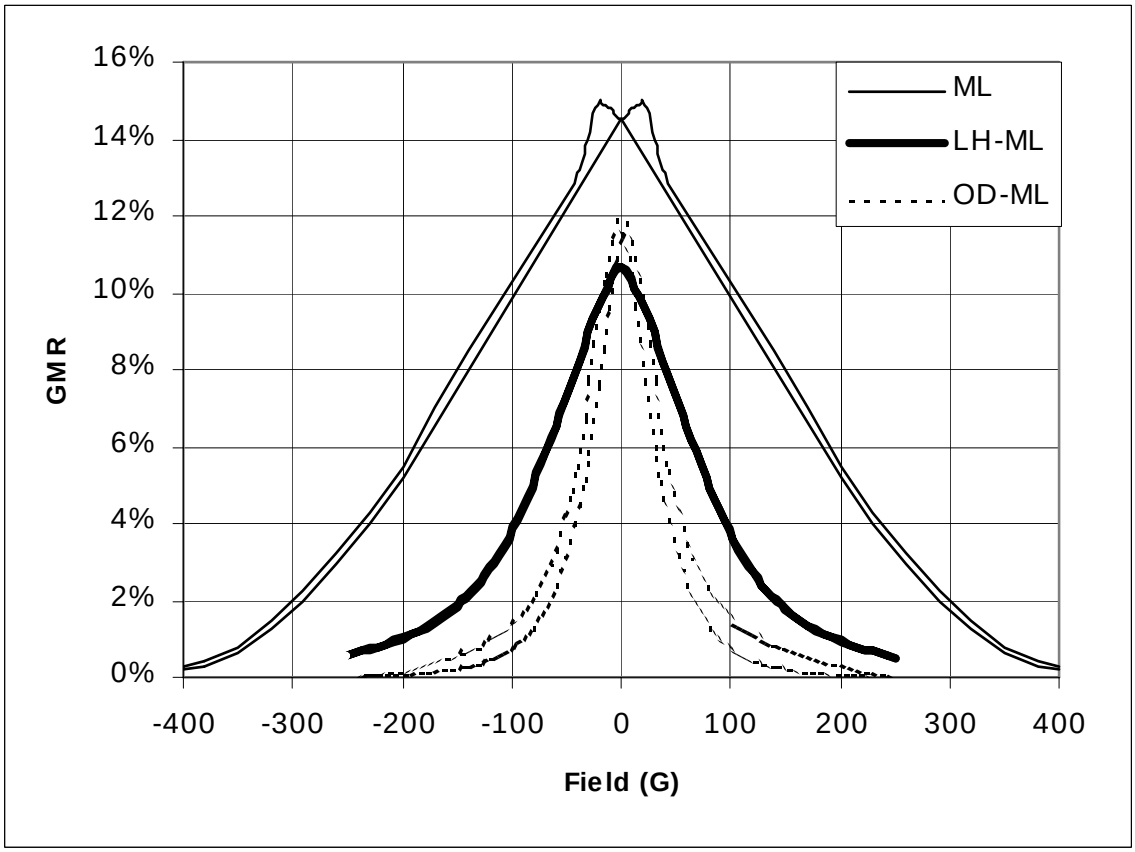

Figure 13. MR traces of GMR *vs*. applied field for conventional multilayer (ML), low-hysteresis multilayer (LH-ML), and high-sensitivity multilayer (OD-ML) materials.

Sensor arrays were also fabricated by gluing individual sensor die to a printed circuit board and die bonding the sensors to the board. In this way an 8-element array of commercial high-sensitivity sensors was provided to Albany with 0.5 mm spacing and a total active width of 4 mm. The results are in the section on results from the period of the program extension.

A variety of spin-dependent tunneling (SDT) sensors were used in this program, most of them were developed under other programs and made available to this program. The most recent development is shape-biased SDT sensors

The SDT junctions are fabricated in pairs and then strung together electrically to make legs of a Wheatstone bridge. Each junction has ferromagnetic top and bottom electrodes separated by an Al_2O_3 tunnel barrier. The key magnetic design feature that is relevant to the low power SDT sensor is the long and narrow shape, and the detailed sequence of layer deposition and annealing in applied fields. The structure of a pair of junctions is schematically shown in Figure 14. The antiferromagnetic (AF) CrPtMn layer has its magnetization direction shown by the pair of antiparallel arrows. This direction is determined during deposition and field annealing. The direction of the moment of the AF layer is coupled to an artificial antiferromagnet (AAF) consisting of two layers of CoFe separated by a thin layer of Ru. Since the magnetic layers are paired with no net moment, it is very difficult to upset them with an external field. The shape bias of the elongated bottom free layer orients its moment in the long direction (perpendicular to the pinned layer) in the absence of an external field. With an external field applied, the moment of the free layer follows the external field resulting in increased or decreased magnetoresistance depending upon the direction.

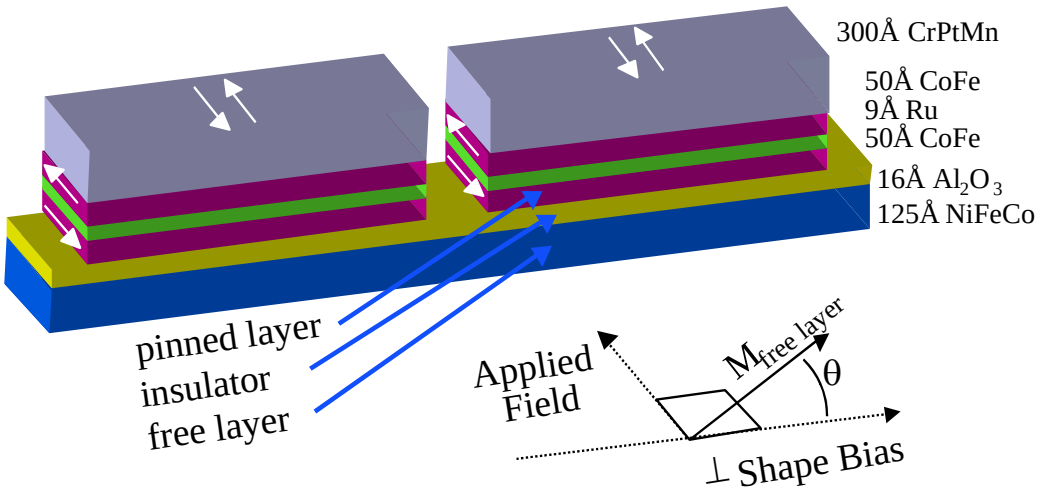

Figure 14. The shape biased SDT junction pair with the detailed magnetic layer structure indicated. Arrows indicate the direction of the magnetic moment of magnetic layers.

The relative direction of the magnetic moments is shown superimposed on an idealized magnetoresistance curve in Figure 15. The initial perpendicular orientation between the pinned and free layers results in a bipolar sensor that can distinguish between positive and negative fields. Note the bottom scale.

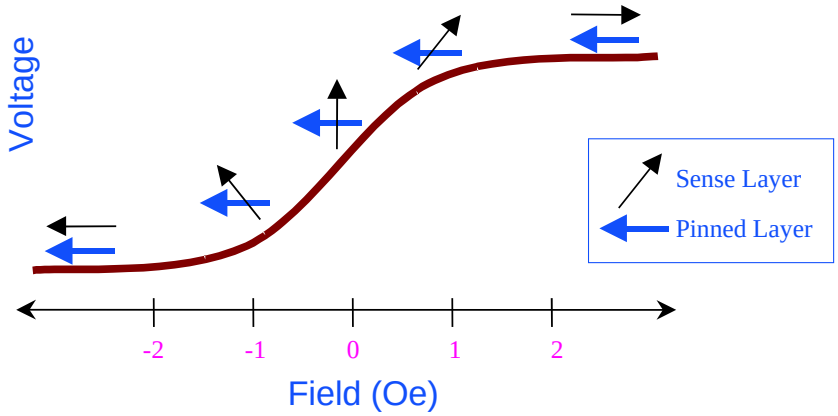

Figure 15. Relative magnetization directions of the free or sense magnetic layer and the pinned magnetic layer superimposed on an idealized curve of voltage vs. applied field for a self-biased SDT sensor.

The MR response curve of one of these shape-biased sensors is shown in Figure 16. The sensitivity in the center of the curve is 195 mV/Oe with an excitation of 5 volts or 39 mV/V-Oe. The material from which these sensors were fabricated had magnetoresistance ratios below 40%. New SDT materials have been recently deposited with over 70% MR ratios promising even more sensitive SDT sensors. NVE has also produced SDT sensors without shape bias with sensitivities as high as 100 mV/V-Oe.

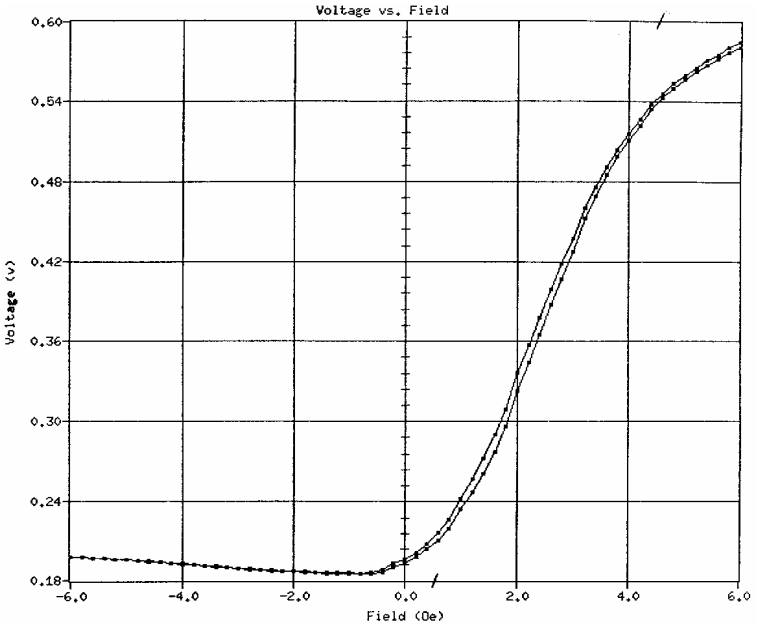

Figure 16. Output of a new shape biased SDT sensor. The sensitivity in the center of the curve is 195 mV/Oe with an excitation of 5 volts or 39 mV/V-Oe.

Throughout the project, we have greatly increased the resolution and sensitivity of GMR and SDT sensors. At the beginning of the project, commercial one-axis GMR sensors with 4 mV/V-Oe sensitivity collected the field from a region 3.0 mm long. Commercial GMR sensors with 10 mV/V-Oe sensitivity are now available. We have X-Y GMR sensors that collect the field from a region of less than 1/4 mm with a sensitivity of 0.7 mV/V-Oe and X-Y sensors that collect the field from a region of 0.8 mm with a sensitivity of 2 mV/V-Oe. With larger flux concentrators, an increase in sensitivity to 10 mV/V-Oe can be achieved with an increase in active sensing area to 2 mm by 2 mm.

The MR ratio of SDT sensors has also steadily increased during the project. Whereas 40% change in resistance was the best a year ago, 70% has now been measured on SDT wafers.

Table I below summarizes the improvements in sensors during this project. Future sensors are indicated with goals.

Table I. Improvements in SDT and GMR sensors during project.

	Sensor type	Sensitivity (mV/V-Oe)	Active Area (mm)
Original	SDT 1 axis	25	2.4x1
Present	SDT 1 axis	100	2.4x1
Shape biased	SDT 1 axis	40	2.4x2
Future	SDT 2 axis	50 ?	?
Original commercial	GMR 1 axis	4	3.0x0.4
Original commercial	GMR 1 axis	1	1.2x0.4
Present commercial	GMR 1 axis	10	3.0x0.4
Present commercial	GMR 1 axis	4	1.2x0.4
Present	GMR 2 axis	2	0.8x0.8
Present	GMR 2 axis	0.7	0.25x0.25
Future	GMR 2 axis	10	2x2

2. Surface Crack Detection

High-resolution probes using the two directional GMR eddy current sensor were used to assess the resolution limits for small defect and surface feature recognition. It was demonstrated that pinholes as small as 0.2 mm diameter (barely visible by eye) and 0.2 mm depth could be reliably detected.

The specimen was an aluminum disk of diameter 24 mm and thickness 9 mm. Onto one surface of the disk, three cracks, of lengths 2, 3 and 1 mm, and a hole, of diameter 0.2 mm, have been machined. All defect had a depth of 0.2 mm. The sizes of the features were chosen as being representative of ‘small’ defects at the limits of delectability for commercially available eddy current probes.

The probe consisted of a flat pancake type excitation coil having an outer diameter of 0.7 mm (mean diameter of 0.35 mm) bonded on to the top surface of a 2-D GMR sensor package. The sensing element consisted of a GMR two-directional sensor (containing a 3:1 flux concentrator), which is capable of monitoring two orthogonal magnetic field components essentially at the same point (over an area of 0.1 by 0.1 mm). The excitation frequency was 100 kHz. A photograph of a similar probe having a 1 mm diameter excitation coil is shown in Figure 17.

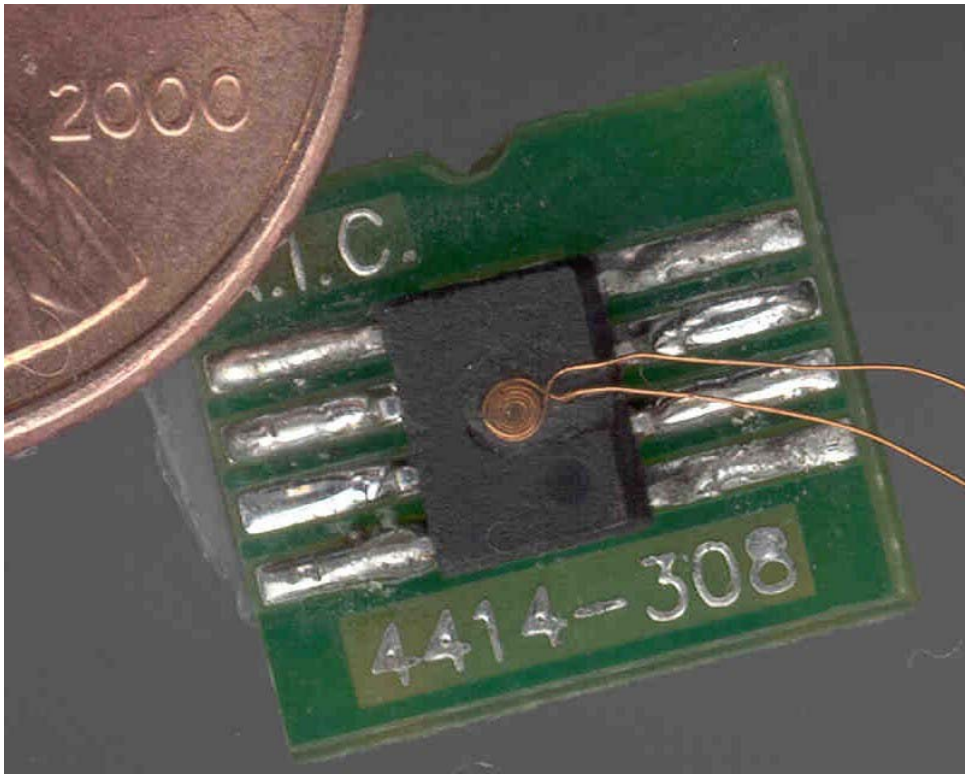

Figure 17. Photograph of the high-resolution GMR eddy current probe.

Experiments were performed on very small defects, by using high-resolution, GMR-based eddy current probes. The probe was scanned over the central area of the specimen containing three cracks of 2 mm, 3 mm, and 1 mm in length, and a small hole of 0.2 mm diameter and 0.2 mm depth. All cracks have the same width (0.2 mm) and the same depth (0.2 mm). The lift-off distance was varied from zero to greater than the diameter of the coil.

Figure 18 shows an eddy current image representing the magnitude output of the sensor when the probe was scanned very close to the surface (0.05 mm lift off). The map on the left shows the output of the sensor that is oriented parallel to the crack orientation (along *y*-axis in the figure). The map on the right shows the magnitude output of the other sensor (perpendicular on the crack direction).

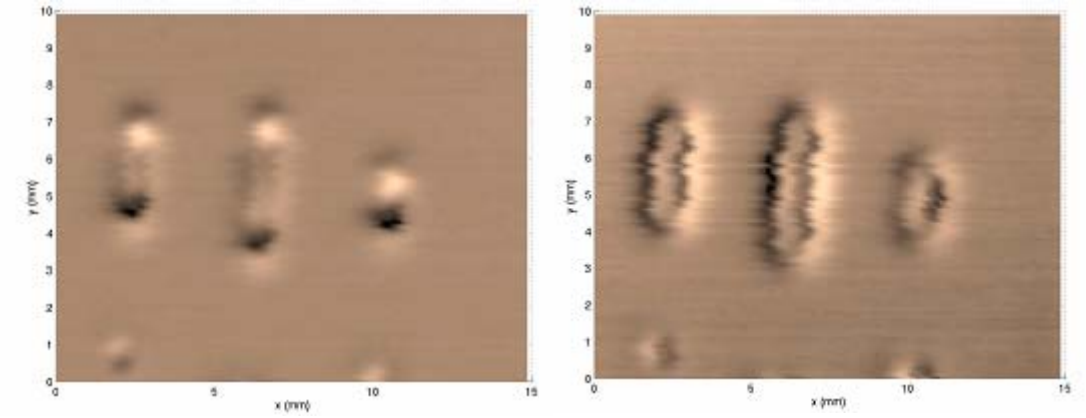

Figure 18. Magnitude map of GMR probe obtained by scanning the central region of the aluminum disc surface (the map of the 0.2 mm hole can be observed in the lower left corner) - sensor. The axis of sensitivity is parallel to the crack direction on the left and perpendicular to the crack direction on the right.

Figure 19 shows the magnitude of the output resulting from combining the output of the perpendicular sensors (the in-plane magnetic field vector magnitude). From these eddy current images, it can be shown that the small pinhole of 0.2 mm (left-corner in the maps) is clearly visible. To demonstrate the effect of the lift off, the map on the left represents a lift off of 0.1 mm and the one on the right represents a lift off of 0.5 mm. It can be shown that the small pinhole can be barely seen on this map. Repeating the measurements at higher lift-off distances, it was observed that the limit of detection of the cracks occurs around 0.8 mm, which roughly corresponds to the diameter of the excitation coil.

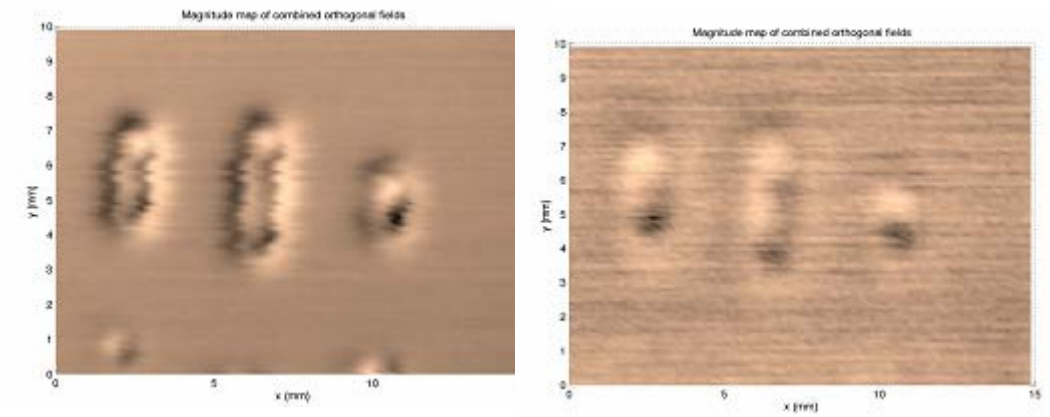

Figure 19**.** Magnitude map of the combined orthogonal fields measured by the 2-D GMR sensor at lift-off distances of 0.1 mm (right) and 0.5 mm (left).

3. Detecting Cracks around Holes in Multilayered Structures

For an experimental study of “multiple origin” corner-crack detection in multi-layered structures, the specimens consist of a stack of identical aluminum plates of thickness 3.2 mm (0.125 in.). The plates have the width of approximately 50 mm (2 in.) and the length of 280 mm (11 in.). Ten holes of 6.3 mm (0.25 in.) diameter were drilled in each plate along the longitudinal symmetry axis of the plate. The distance between the centers of adjacent holes is 19 mm (0.75 in.).

Various transverse notches initiating from the edge of different holes were machined. The lengths of notches range from 1 mm (0.04 in.) to 2.5 mm (0.1 in.). All notches have the same height of 1 mm (0.04 in.). Note that the height of the cracks is less than one third of the thickness of the plate, emulating corner cracks.

The design of the probe takes into consideration the need for a fast scanning inspection method. Linear scanning is preferred to the circular scan around each hole. The geometry of the probe and the scanning of the specimen are shown in Figure 20. The GMR sensor is placed on the longitudinal axis of the coil, with its sensitive axis perpendicular to the current lines. When the probe is scanned along the longitudinal axis of the specimen, the probe’s output is theoretically zero due to the symmetry of the magnetic field at the sensor location, A crack on one side of a hole breaks the symmetry of the field, producing a non-zero sensor output.

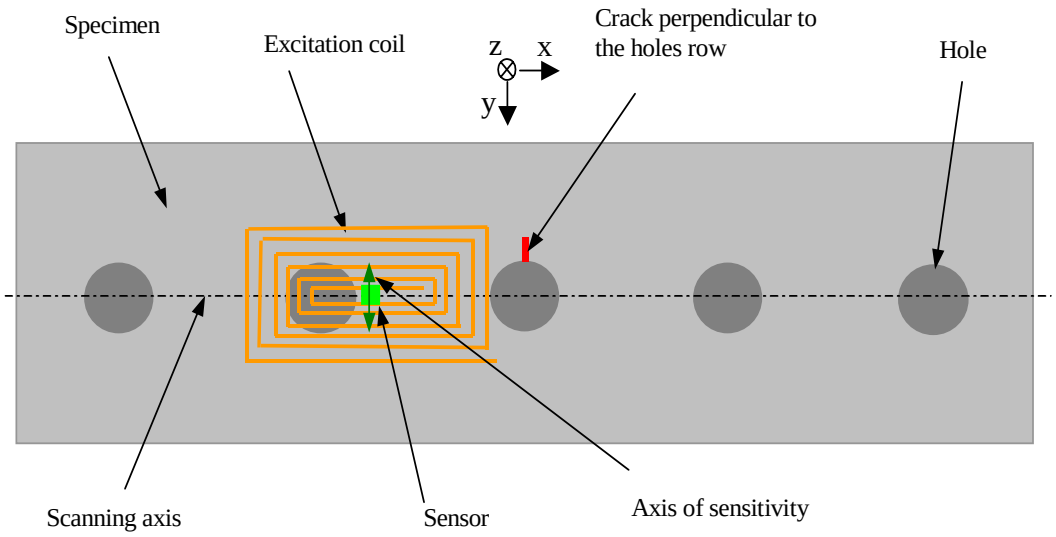

Figure 20. Detection of transverse cracks using a probe with a flat linear coil of rectangular shape and a central GMR sensor scanned along the fasteners row axis.

The plate containing two defects -- hole #3 and hole #7-- was scanned when the defects were at the upper surface of the plate (surface defects). The current amplitude through the coil was 2.5 A. For the surface defects an excitation frequency of 10 kHz was chosen. The probe was aligned such that the ripples in signal produced by defect-free holes were minimized, when the probe was scanned along the axis of the row. To further enhance the defect detection capability, the signal produced by defects was "filtered" from background signals (coming from the hole's edge or from misalignments within the probe) by monitoring the out-of-phase component (Y signal) of the lock-in amplifier. The phase of the reference signal generated by the lock-in amplifier was adjusted until the background signals were minimized. For surface defects, the reference phase was 0 degrees. Figure 21 shows the out-of-phase signal when scanning the whole length of the plate (along the axis of the row). The left notch in hole #3 (2.5 mm in length) produced a positive peak, while the right notch in hole #7 (2 mm in length) – a negative peak. Because the scanning was manual, the scanning speed could not be maintained constant. Consequently, the positions of peaks (or of the ripples corresponding to the defect-free holes) do not correspond precisely to the positions of holes indicated in Figure 21.

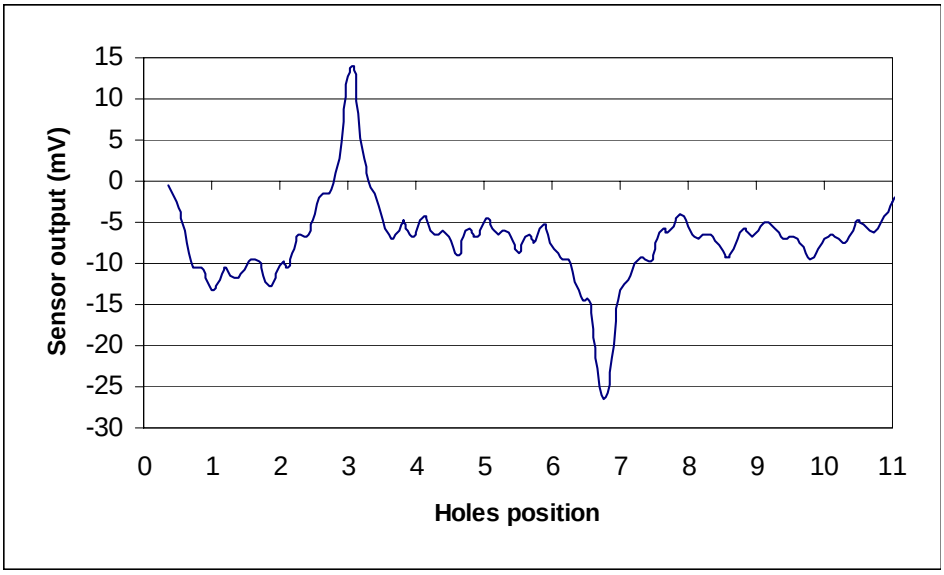

Figure 21. Out-of-phase signal from the sensor when the probe is scanned along the specimen containing the defects (in hole #3 and hole #7) at the top of first layer (surface defects).

In the second experiment the plate was flipped to the opposite side such that the notches are at the underside of the plate (the upper edge of defects being at a depth of 2.2 mm below the surface). The probe was scanned along the axis of row, at different excitation frequencies. The optimal detection was achieved at a frequency of 2 kHz, and a reference phase of 25 degrees – see Figure 22.

Because the plate was flipped, the crack of hole #3 became right-side crack, resulting in a negative peak. Observing the relatively high background signal and high amplitude ripples caused by defect-free holes, we conclude that the alignment of the probe for this measurement was poorer than for the first measurement (surface defects). However, the defects are clearly visible in the graph of Figure 22.

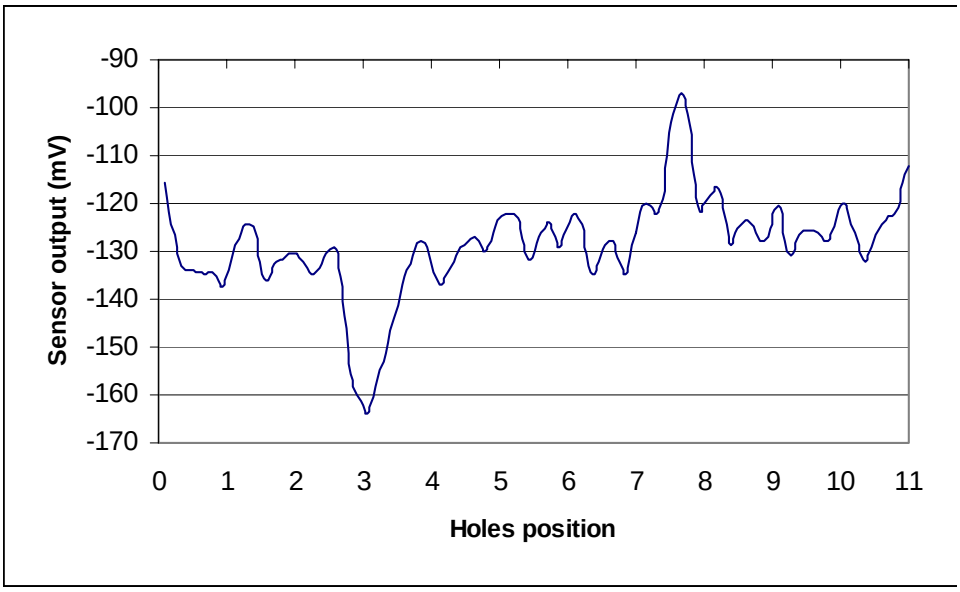

Figure 22. Out-of-phase signal from the sensor when the probe is scanned along the specimen containing the defects (in hole #3 and hole #7) at the bottom of first layer (2.2 mm below the surface).

A second specimen containing shorter defects, between 1 mm and 2 mm in length, was also tested.

The probe was scanned above the longitudinal axis of the two specimens, with the defects at the bottom of the plates (buried defects at 3.2 mm depth). For optimum detection, the excitation frequency was 2 kHz. The out-of-phase output of the lock-in amplifier is shown in Figure 23 for the first specimen, and Figure 24 for the second specimen. The left-side notches were detected as negative peaks, while the right-side notches were detected as positive peaks. It can be noticed that the shortest notch of 1 mm in length (in the second specimen, hole #5) can be clearly distinguished in Figure 24. The amplitude of the signal from this defect is approximately 4 times larger than the background signal coming from defect-free holes.

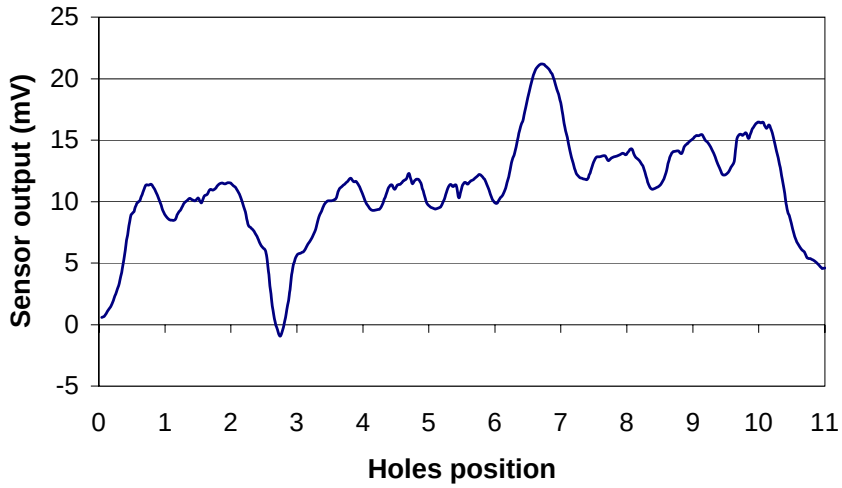

Figure 23. Out-of-phase signal from the sensor when the probe of Figure 20 is scanned along specimen 1 containing defects (at hole #3 and hole #7) at the bottom of the 3.2 mm thick plate.

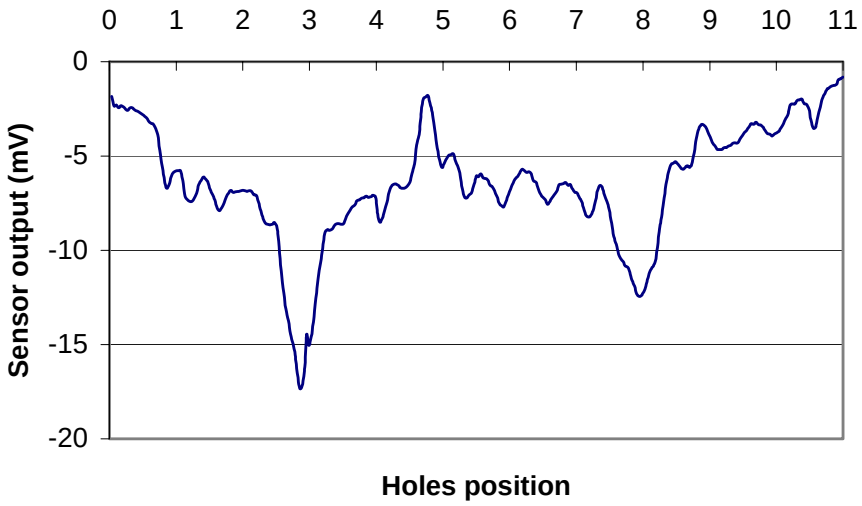

Figure 24: Out-of-phase signal from the sensor when the probe of Figure 20 is scanned along specimen 2 containing defects (at holes #3, #5 and #8) at the bottom of the 3.2 mm thick plate.

These results show that corner cracks as small as 0.5 mm around holes in multilayer structures can easily be detected to a depth of 3.2 mm by these single-sensor eddy-current probes.

To increase the depth capability of these probes, Albany Instruments developed an original eddy current technique, similar to the remote field eddy current method, using flat linear coils and GMR sensors. This technique has been successfully applied to detect cracks around fastener holes located on the backside of the specimen (deeply buried flaws) up to 4.8 mm depth.

The new eddy current technique uses the returning magnetic flux created by the excitation coil, external to the coil, to create eddy currents remote from the coil area, on the backside of the specimen. In general, the returning field is much weaker than the internal main field, because it is spread over a larger area around the coil. In the case of a specimen containing fastener holes, the holes provide a path for the returning magnetic flux to close with their source. The holes act as magnetic flux concentrators for the returning flux. Consequently, circular eddy current of significant intensity can be induced on the backside of the plate, around the fastener holes. By placing the detecting element above the hole, and remote from the excitation coil, the backside cracks around holes can be reliably detected.

Figure 25 shows the principle of this method for detecting backside cracks in a row of fastener holes. Two flat rectangular coils, made on the same ribbon cable, are symmetrically located on the two sides of the row of fasteners. The current in the two coil flows in the same sense (counterclockwise in Figure 25). The flux inside both coils has the same direction, as indicated in Figure 25 (perpendicular to the coil plane). These fluxes travel through the thickness of the specimen, being attenuated by the eddy current field created into the specimen, under the coils areas. However, if the frequency is chosen low enough such that the excitation magnetic field is not totally canceled by the eddy current field, there will be a magnetic flux on the opposite side of the specimen. This magnetic field is focused by the hole to return to the surface the specimen (the magnetic field lines of the coils are closed loops). Because the area of the hole is small compared to the length of the coil, the holes will act as flux concentrators for the returning flux. The returning flux (shown in Figure 25 as a arrow perpendicular to the specimen surface – in the opposite direction to the excitation flux) will create significant eddy currents around the hole on the backside of the specimen. The eddy currents around the hole will be attenuated towards the surface of the specimen. Therefore, this probe is only suitable for detecting deeply buried flaws on or near the backside of the specimen. Note that the excitation coils are placed far enough from the hole region, such that no eddy currents are created around the holes at the surface. As a consequence, this probe is not capable of detecting surface or near surface cracks around holes.

For optimal detection of transverse cracks (perpendicular to the row axis), the GMR sensor will be placed between the two coils, being scanned along the axis

of the fasteners row. The sensitive axis of the sensor is oriented perpendicular to the axis of the row – see Figure 26.

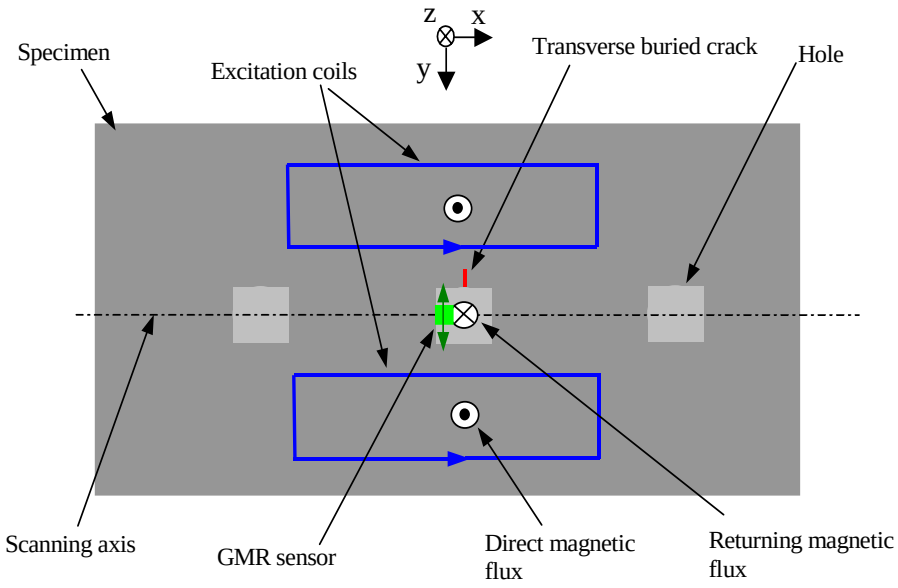

Figure 25. Remote-field eddy-current probe for the detection of buried transverse cracks using a probe based on two rectangular coils and a GMR sensor. The sensitive axis of the sensor is perpendicular to the scanning direction. The probe is scanned along the axis of the fasteners row.

A three-coil based probe can provide a solution for detecting both surface cracks and deeply buried cracks. The third rectangular coil is placed between the two coils of the probe described above (on the same ribbon cable), with the current flowing in opposite direction to the flow in the other two coils (clockwise in Figure 26). With this configuration the magnetic flux through the hole is enhanced, because the returning flux from the two coils will add to the main flux of the third coil. In addition, surface and near-surface cracks can be easily detected due to the eddy currents created by the third coil at the surface. The current experimental study showed that this three-coil configuration enhances the detection capability of deeply buried cracks (as compared to the two-coil probe presented in Figure 25 and to the one-coil probe presented in the previous progress report).

The probe configurations shown in Figures 25 and 26 were manufactured on the same ribbon cable. Three flat, spiral rectangular coils were configured using jumper cables to connect the appropriate ends of the ribbon wires. The central coil (see Figure 26) has 10 turns and a mean diameter of 6 mm – 20 wires were connected over a width of 12 mm. The two symmetrical, lateral coils were placed adjacent to the central coil. They have 8 turns each and a mean diameter of 11 mm. By properly connecting the ends of the coils, the two-coils configuration of

Figure 25 and the three-coils configuration of Figure 26 were obtained on the same ribbon cable. By connecting only the central coil the configuration described in previous progress report is obtained. This flexible design enabled us to directly compare the performance of the three probe designs.

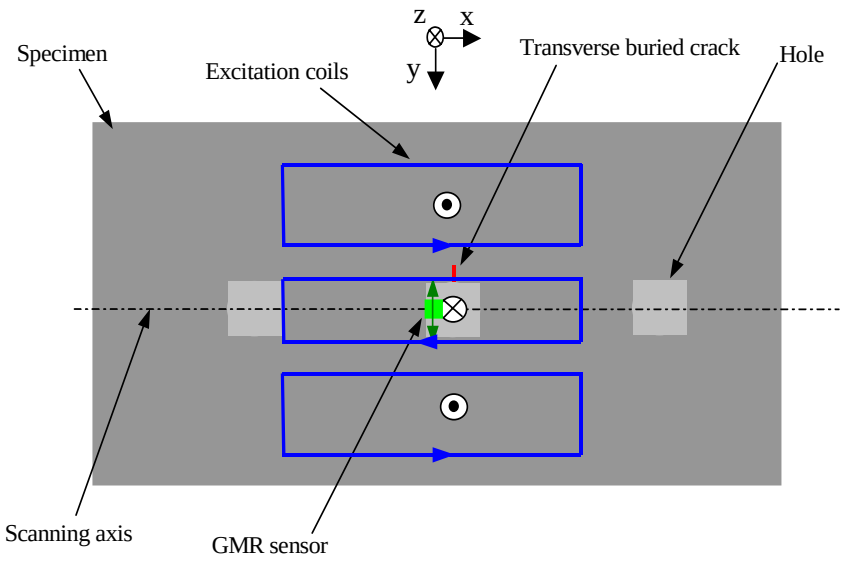

Figure 26. Combined "reflection – remote field" eddy current probe for the detection of transverse cracks using a probe based on three rectangular coils and a GMR sensor. The sensitive axis of the sensor is perpendicular to the scanning direction. The probe is scanned along the axis of the fasteners row.

The probe was manually scanned along the specimen containing 2 cracks in hole #3 (2.5 mm long) and hole #7 (2 mm long). Firstly, the two-coil probe shown in Figure 24 was scanned along the specimen axis, with the cracks on the backside of the plate (3.2 mm under the surface). The excitation frequency was 2 kHz. The out-of-phase component of the sensor's output is shown in Figure 27. The results are comparable to those obtained using a single central coil in terms of crack signal to background (hole) signal ratio. By scanning the three-coil probe a slightly improved crack/background ratio was obtained as shown in Figure 27.

Subsequently, a plate of thickness 1.6 mm was placed on the top of the specimen to test the capability of detection of defects buried at 4.8 mm below the surface. The result obtained using the three-coil probe at a frequency of 1 kHz is shown in Figure 28. In this figure it can be observed that the crack signal is

about three times larger than the background signal caused by the defect-free holes. The other two probes (central coil probe, or two-coil probe) showed a poorer capability of detection of the cracks at this depth (ratio lower than 2:1 were obtained).

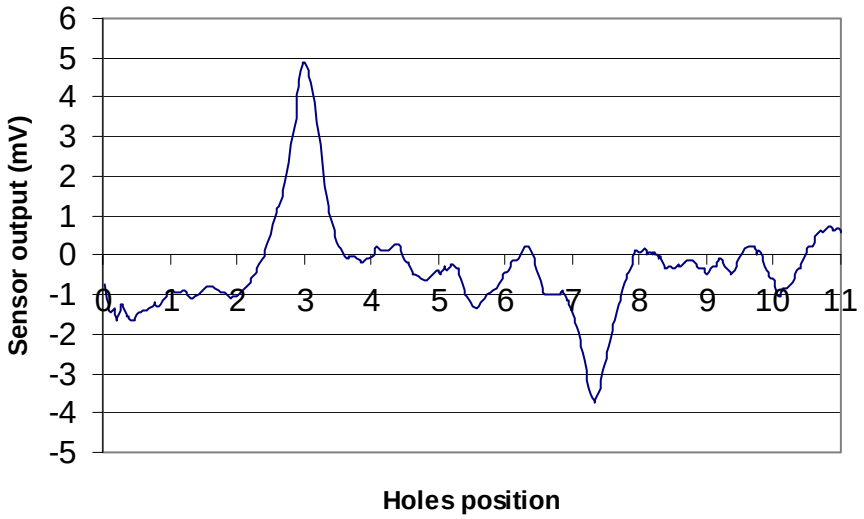

Figure 27. Out-of-phase map of the remote-field eddy current probe when scanned along a specimen containing two cracks of 2.5 mm (hole #3) and 2 mm (hole #7) respectively, at 3.2 mm depth.

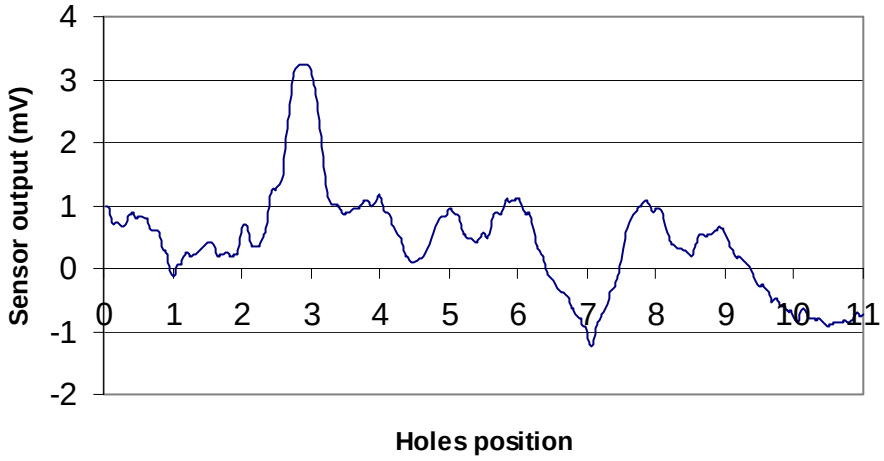

Figure 28. Out-of-phase map of the combined “reflection – remote field” eddy-current probe when scanned along a two-layer specimen containing two cracks of 2.5 mm (hole #3) and 2 mm (hole #7) respectively, at 4.8 mm depth.

In conclusion, the combined “reflection-remote field” eddy-current probe shows superior performance for detecting deeply buried flaws in multi-layer structures. Because the excitation coils are located outside the area of fastener holes, the new remote-field eddy-current probe can be used in applications where the fasteners have protruding heads. These applications would require a high lift off of the excitation coils in the case of traditional reflection probes. By increasing the lift off the capability of detection of deeply buried cracks is reduced. With the remote excitation, the coils can be scanned much closer to the specimen surface, enhancing the probe sensitivity.

4. Corrosion Detection

The performance of GMR eddy-current probes for detection of subsurface corrosion was assessed. For this experiment, pinholes of small diameters (0.75 mm) of different depth were detected on the backside of an aluminum layer of 1.6 mm thickness. A 0.75 mm diameter, 0.25 mm deep, pinhole that represents 15% of the plate thickness was clearly detected using our GMR eddy-current probes. The experiment was repeated using the new portable eddy-current system developed at Albany. The results were comparable to the ones obtained using standard instrumentation.

The goal of the experiment was to detect these simulated corrosion defects from the opposite side of the plate. To obtain the penetration depth and the resolution required for this type of defects, an excitation coil of mean diameter of about 2 mm was chosen. The flat circular excitation coils used in subsequent experiments contained 24 turns, disposed in two 2 layers (the external diameter was 3.6 mm). An alternating current of 0.54 amperes peak amplitude was passed through the coil. The optimum detection of defects was obtained at the frequency of 8 kHz. A schematic diagram of the location of the probe above the specimen during the experiment is shown in Figure 29.

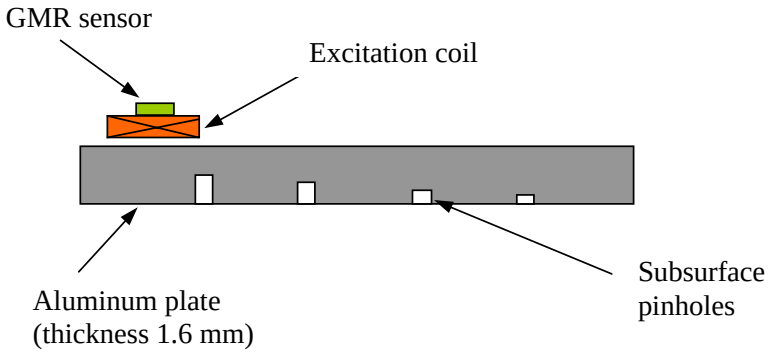

Figure 29. Schematic diagram of the experiment to detect hidden corrosion in metallic layers.

First, a raster scanning covering the region of both rows of holes was performed. The magnitude and phase maps obtained are shown in Figure 30a and 30b. It can be observed that all buried holes are clearly visible in both plots. The smallest holes (0.25 mm depth) are better visible on the phase plot. The results of a single scan (at the same frequency – 8 kHz) along the median line of each row are shown in Figure 31. In this plots the out-of-phase output of the sensor is represented.

a.

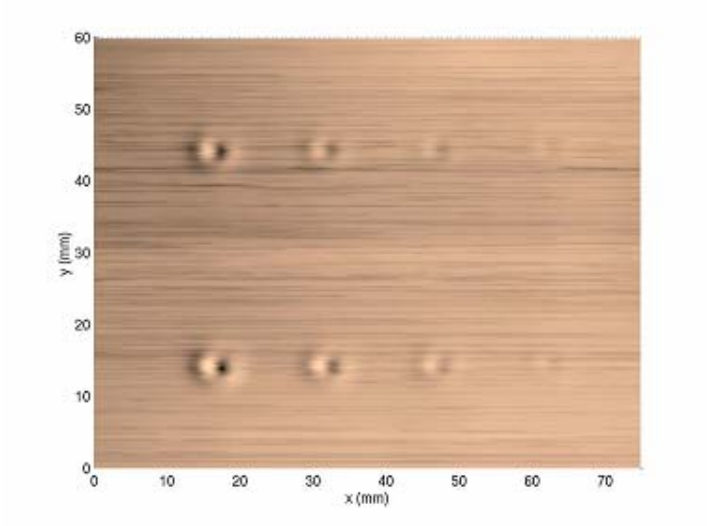

b.

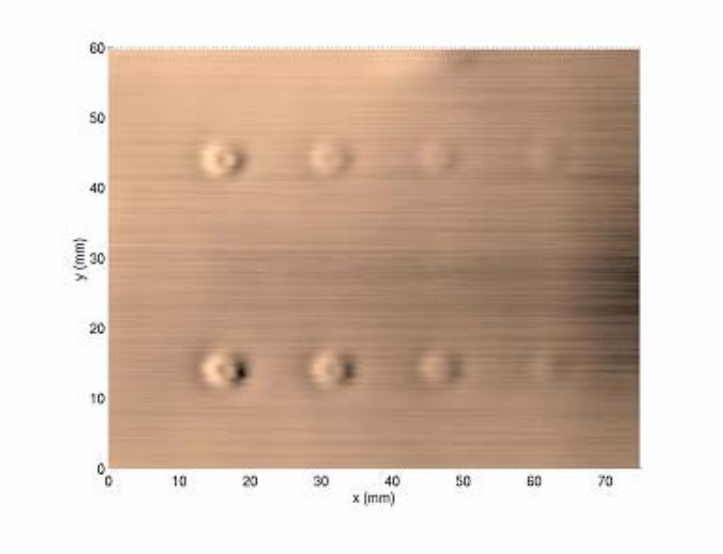

Figure 30. Maps of the Magnitude (2a) Phase (2b) of the sensor output from a two-dimensional scan of a specimen containing subsurface holes. The excitation frequency was 8 kHz.

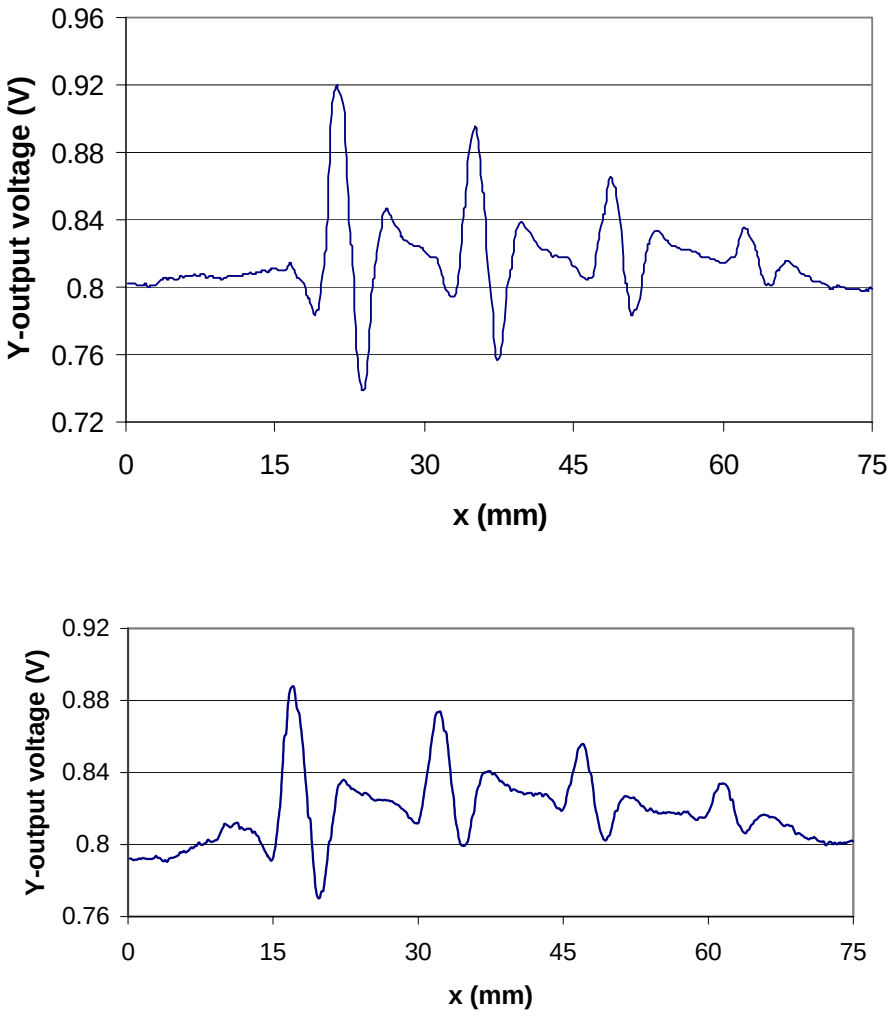

Figure 31. Out-of-phase output of the sensor for one scan of the 1 mm diameter holes row (above) and of the 0.75 mm diameter holes row (below). The excitation frequency was 8 kHz.

Finally, a single scan along the row of 0.75 mm diameter holes was repeated using the portable eddy current system developed at Albany. This system eliminates the standard lock-in amplifier by using a laptop computer with a digitizer card and software that emulates a lock-in amplifier. For this experiment the frequency of the excitation current provided by the computer was 2 kHz (which is close to the upper frequency limit of current portable system). The out-of-phase output of the sensor is shown in Figure 32.

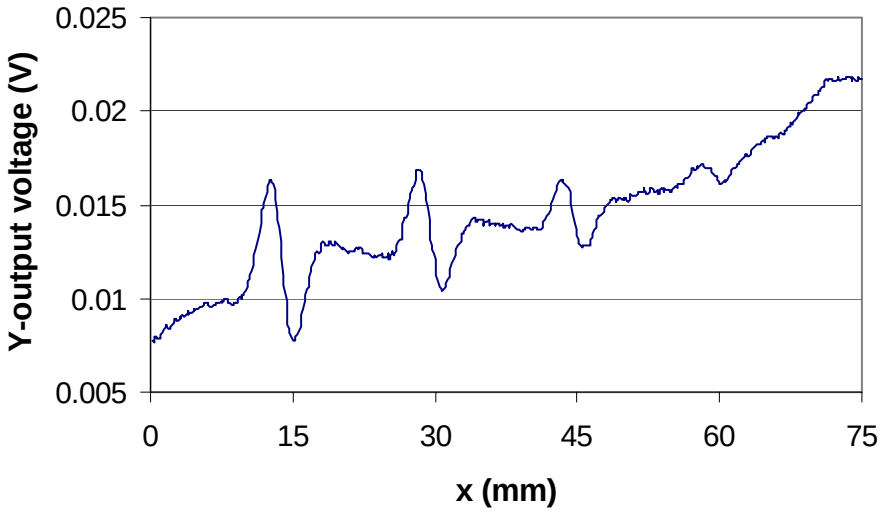

Figure 32. Out-of-phase output of the sensor for the scan of the 0.75 mm diameter holes using the portable eddy current system. The excitation frequency was 2 kHz.

The ability to detect surface corrosion, especially when under a dielectric coating is another important problem. To show the ability of GMR-based eddy-current probes to detect small surface irregularities such as corrosion, eddy-current scans of coins were done. These scans demonstrate the resolution of an eddy current probe to small surface irregularities.

In the Phase I program a map of the coin profile was obtained by scanning the probe over the coin using a coordinate measuring machine. A sinusoidal current of 1.3 A amplitude at a frequency of 100 kHz was passed through the excitation coil. The lift-off separation between the coil and the coin surface was 0.1 mm. Data points were measured using a square grid with steps of 0.1 mm in both directions, such that we obtained 250x250 pixels (data points) for each 25 mm x 25 mm map.

The resolution of the probe at that time was somewhat better than 1 mm as indicated in the image in Figure 33. Improved GMR sensors and GMR-sensor based eddy-current probes developed in the Phase II program has improved the resolution to the point that the letters can be read as shown in Figure 33.

A probe comprising a 2-D high-temperature GMR sensor and a 6-turn excitation coil of external diameter 0.7 mm was used for these experiments. The excitation current was provided from the internal source of the Perkin-Elmer Model 7280 lock-in amplifier via a current amplifier. An excitation current of amplitude 1.2 A was used in all measurements. The output of the sensor was amplified by using a SR560 low noise preamplifier with the cut-off frequency of 1 MHz. The output of only one sensor (sensitive along x-axis) was monitored. The output of the

lock-in amplifier was recorded in terms of R (magnitude) and Θ (phase). Figure 34 shows the phase map of the coin at the frequency of 900 kHz.

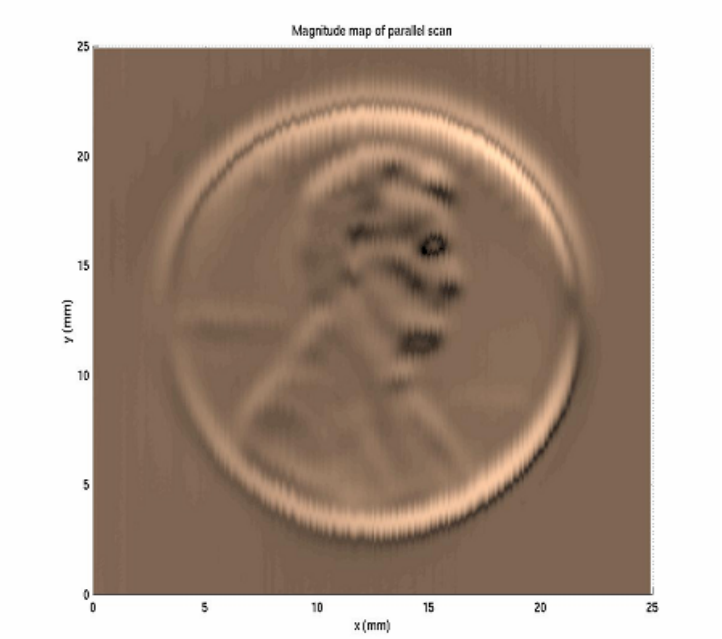

Figure 33. Eddy current map of a US penny obtained at 100 kHz using a commercial GMR sensor.

Figure 34. Eddy-current phase map of a US penny obtained at 900 kHz with using an X-Y GMR sensor using high sensitivity GMR material.

5. Integrated Eddy-Current Probe and Portable System for Small Surface Cracks

Albany Instruments development of a new portable eddy current system for low frequency applications. The data acquisition program uses LABVIEW software

The Labview program comprises two major modules:

1. Generation of two sinusoidal waveforms having the phases shifted at 90 degrees (in quadrature). The user can adjust the frequency, amplitude and initial phase of two waveforms (sine & cosine).
2. Data acquisition module that acquires the signal from the sensors, and performs the multiplication of this signal with the sine- and cosine waveforms generated by the first module. The resulting waveforms are subsequently low-pass filtered to extract their DC components that represent the "in-phase" (X) and the "quadrature" (Y) components of the sensor's output. The results are displayed in real-time on the control panel of the Labview acquisition program and are saved in data files that can be represented as 2-D or 3-D graphics using Excel or Matlab.

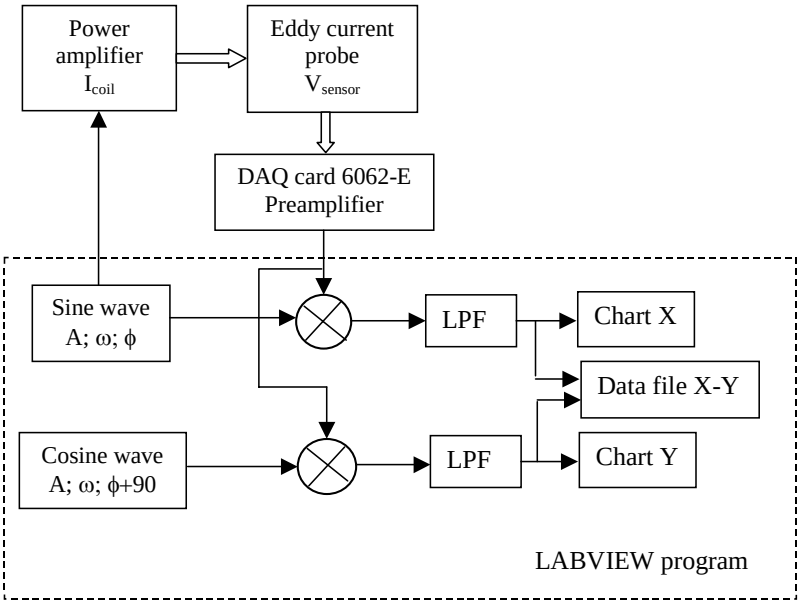

Figure 35. Block diagram of the portable eddy-current measurement system.

The block diagram of the measurement system is shown in Figure 35. The full circuit has been implemented using VI's blocks available in Labview (version 6.1), such as analog input VI's, analog output VI's, waveform multiplication VI's

and DC averaging VI's (that performs the extraction of X and Y). For fast acquisition more advanced techniques (based on intermediate analog input and analog output VI's) have been used.

In order to obtain continuous generation of the sinusoidal waveforms and continuous acquisition from the sensor output, circular buffering technique is applied. A simple buffered technique, because of the limited size of the buffer, is not appropriate when a large number of data point at a fast rate need to be acquired. For this type of applications, the circular buffer needs to be used. Using this technique, portions of data are read from the buffer while the buffer is being filled. In this way, the DAQ device continuously acquires data in the background while Labview retrieves the acquired data.

The results using this system for detecting buried cracks around holes disposed in a row were comparable to the results obtained using standard instrumentation. The Labview programs replaced the tasks previously performed by the lock-in amplifier and the sinusoidal signal generator. The software solution represents a significant reduction in cost and size of the eddy current measurement system.

For testing the new portable system, a previous experimental setup was used. The specimen consisted of a plate of 3.2 mm in thickness containing 10 holes. Two cracks are located in hole #3 (2.5 mm long) and hole #7 (2 mm long), on the backside of the plate. The three-coil probe described in the section on Detecting Cracks around Holes in Multilayered Structures has been used for this experiment. The probe was manually scanned linearly along the axis of the row of holes. A digital photo of the experimental setup and the results obtained using a Gateway laptop computer is shown in Figure 36. The compact data acquisition card DAQ-6062E was inserted in the PCMCIA slot of the laptop. The graph shown in the lower part of the computer screen represents the out-of-phase (Y) signal of the sensor. The two-peak signal obtained in this graph indicates the presence of the two cracks (one on left side – the negative peak, and the other on the right side – the positive peak). The results were obtained using a sinusoidal waveform of 1 kHz generated by the computer at one the analog outputs of the data acquisition card. An analog triggering technique was implemented to synchronize the acquisition of the sensor's signal with the sinusoidal waveform sent to the excitation coil from the computer.

The performance of the system in terms of acquisition speed was tested using a Toshiba Satellite laptop (2 GHz). The maximum frequency at which the system can operate is limited by the speed of the analog-to-digital converter of the DAQ card. The DAQ-6062E card has a sampling rate of 500 kS/s. When sampling a periodical signal, one must consider a minimum number of samples/cycle to be acquired in order to obtain an accurate measurement of the amplitude and phase of the signal. By choosing a number of 20 samples/cycle for the acquisition, the system was successfully tested up to a maximum excitation frequency of 5 kHz.

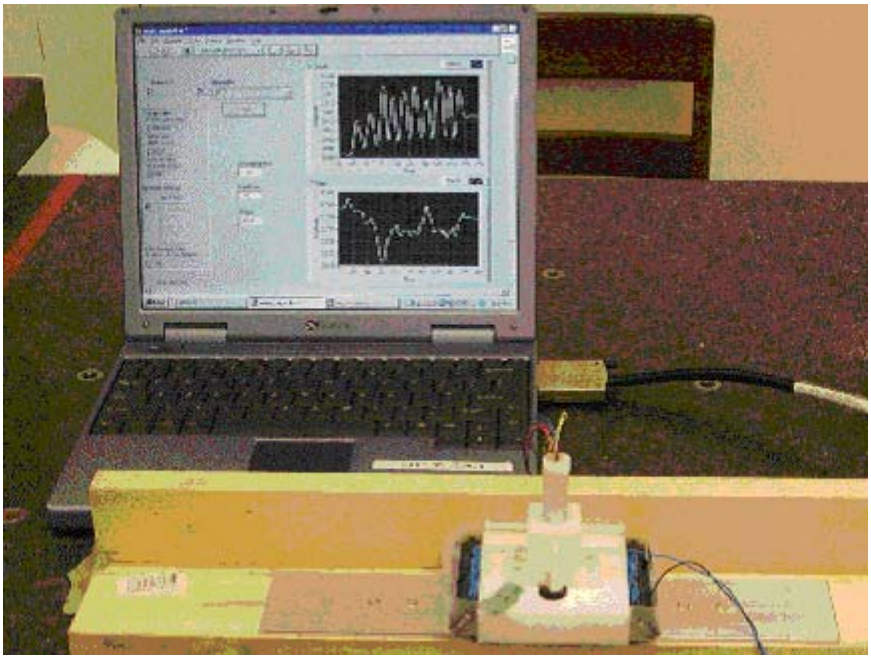

Figure 36. Test results of the portable eddy current system for low frequency applications.

To improve the performance of the portable eddy current system for detecting buried flaws under fastener holes, the standard low-noise preamplifier SR560 was replaced with an integrated instrumentation amplifier AD8225. Having a fix gain of five, the instrumentation amplifier AD8225 does not require additional components to be added on board. The amplifier, having the same size as the GMR sensor (housed in a SOIC package) was placed on a board next to the GMR sensor board within the probe housing. A simple RC high-pass filter has been added to the signal conditioning circuit board to reject the dc component from the sensor output. The dc sensor output component is due to the bias field applied to the sensor in order to obtain maximum sensitivity at small ac fields. The cut-off frequency of the high-pass filter is about 5 Hz. The signal from the transducer is further amplified - up to 100 times - by using the data acquisition card DAQCard-6062E inserted in the PCMCIA slot of the laptop computer. The in-phase and out-of-phase amplitudes of the output signal are extracted using the Labview program described in a previous report. The schematic diagram of the signal conditioning and data acquisition systems of the portable eddy current system is shown in Figure 37.

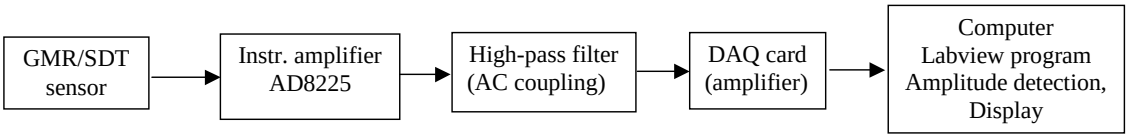

Figure 37. Block schematic of the signal conditioning and data acquisition for the portable eddy current system.

The new portable system incorporating the signal conditioning described above has been tested for the detection of cracks in a row of holes. The experiment has been performed on a specimen of 3.2 mm thickness, containing 10 holes, that has been previously used to test the former eddy current system (comprising standard laboratory instrumentation). Two buried notches are located at the hole #3 (left side) – the 2.5 mm long notch, and at the hole #7 (right side).

A sinusoidal signal of frequency 2 kHz and amplitude of 1 A has been supplied to the flat rectangular excitation coil from the laptop computer. To obtain the optimum crack signals on the out-of-phase map, the initial phase was set at –28 degrees. The out-of-phase sensor output map obtained using the portable system is shown in Figure 38. The map is very similar to the map obtained using standard instrumentation (Perkin-Elmer 7280 lock-in amplifier and Stanford Research SR560 low-noise preamplifier). The ratio between the crack signal and the background signal from defect-free holes is about 5 in both cases.

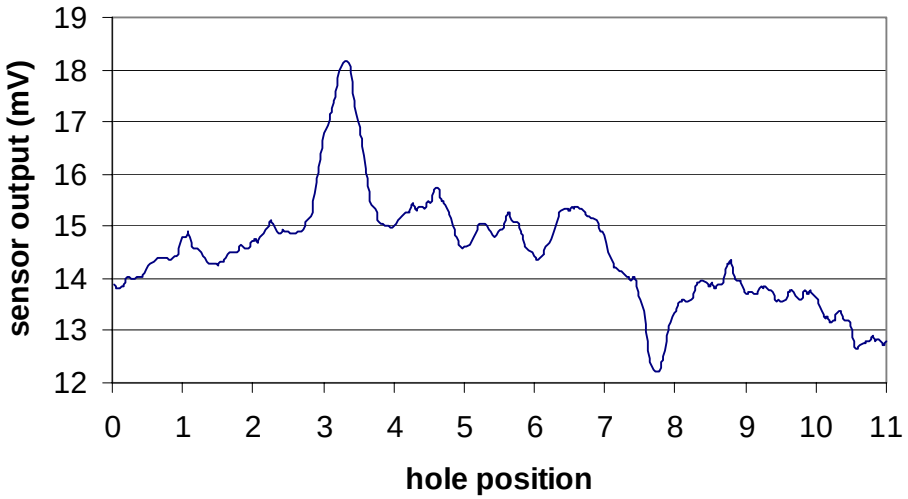

Figure 38. Out-of-phase sensor output from the portable eddy-current system when scanned above the specimen containing notches in holes #3 and #7.

6. Probe Arrays for Rapid Data Acquisition

The processing of data from the 16-element and 8-element sensor arrays described in the section under sensors must be multiplexed for signal processing and display. A multiplexed data acquisition system for monitoring GMR sensor arrays was developed. The original system was aimed towards monitoring of a 16-element array, it is envisaged that this arrangement can be readily extended for the monitoring of larger linear and two-dimensional arrays (i.e. row and column data).

A block diagram of the data acquisition system for monitoring the 16-element array is shown in Figure 39. Two 8-channel multiplexers (AD 7501 & AD 7503) are combined for 16 channel selection. This circuit is made possible by using multiplexers with the same specifications and pin configurations where one of them has an *enable* input that is active 'true' and the other is active 'false'. Because the output impedance is high in the disabled state, the outputs from the multiplexers can be directly connected. The host computer will provide control using a *nonlatched* (no handshaking) digital signal using 4 bits of a single port on the AT MIO16X, series E, data acquisition board. The array that was assessed comprised 16 half bridges with 56-ohm elements spaced at 15 μm. Through resistance of the multiplex switches was approximately 170 ohms with the multiplexer output connected to ground through a 50 kohm resistor. The output of the multiplexers was band-pass filtered and amplified prior to connection to a lock-in amplifier. Finally, the output *X* and *Y* signals from the lock-in amplifier was measured using two ADC channels of the same data acquisition card.

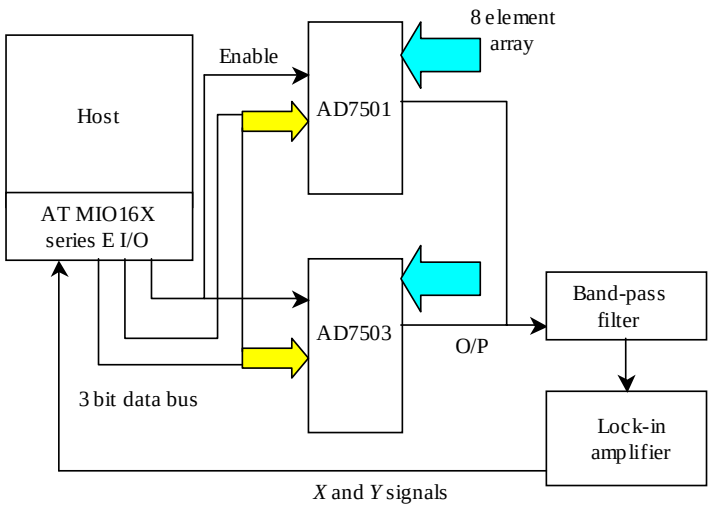

Figure 39. Block diagram of the multiplexed data acquisition system for measurement of the GMR array outputs.

CMOS compatible digital inputs to the two multiplexers were provided from a National Instruments MIO16XE data acquisition card controlled within a Labview software environment. A typical switching time for the multiplexer is around 1 μs, which is considerably faster than the control system used to obtain the experimental results of this report. Through resistance of the multiplexer is typically around 200 Ω, and a 100 kΩ resistor was connected from the output of the multiplexers to ground to provide a finite current sink.

A generic program enables the user to specify the number of readings, a times delay in milliseconds between each reading, a time delay between the measurement of each sensor, and the array size. Each reading corresponds to the measurement of all 16-sensor outputs and the storage of these in an array. Upon running the program, the data is collected at the specified time intervals and saved in a spreadsheet compatible format. When the program is running the current reading is displayed numerically and all the data is also plotted on a waveform chart. Using a rather slow (133 MHz) computer the minimum time to record 80 data points is 12 seconds or approximately 10 ms per sample. With improved computation speeds and changes of the program algorithm, this time can be reduced by factor of 100 or more.

As a demonstration of the multiplexed data acquisition system and to assess the sensitivity of the array elements, a small, permanent magnet was manually traversed along the line of the array. The output from this scan is shown in Figure 40 (the output measurement from sensor 6 has been removed from this plot). While there is a linear variation in the offset between each sensor, it is clear that each exhibits a similar sensitivity. By removing the offset of each sensor it is possible to compare the signal from all 16 sensors in Figure 41. From this plot it is clear that sensor 6 has a significantly lower sensitivity than the other sensors of the array.

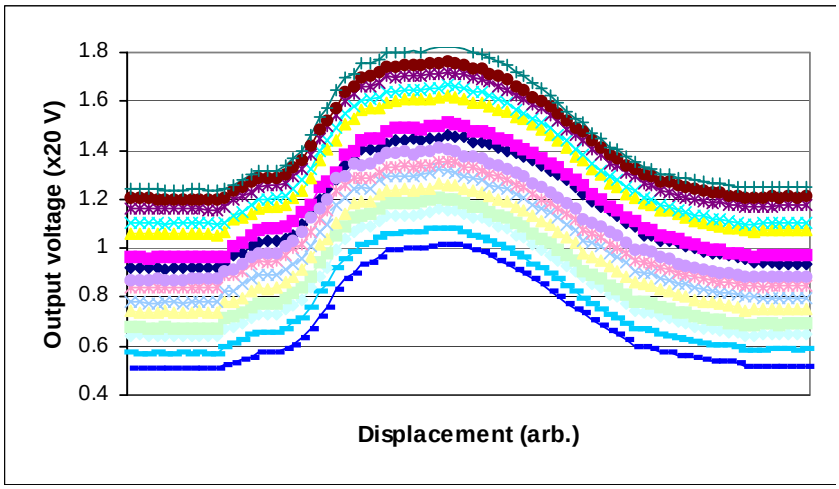

Figure 40. Outputs from the sensor array during the traversal of a permanent magnet in the line of the array. the magnet is remote from the array at each end of the trace.

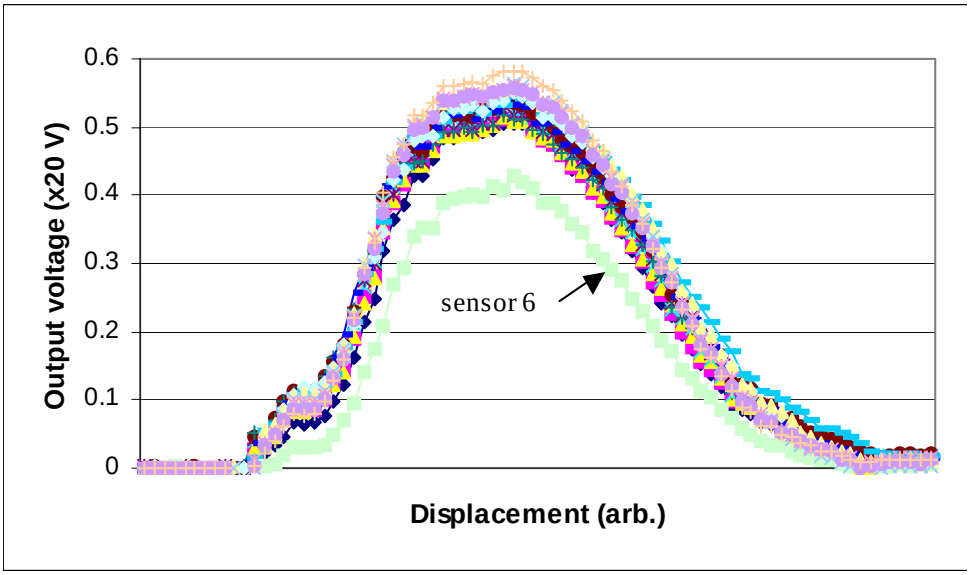

Figure 41. The same data as in Figure 40 with the initial sensor offsets removed

The second data acquisition system was designed for GMR sensor arrays for mapping ac electromagnetic fields. This system can also be used in eddy current testing applications.

The key feature of this system is the parallel processing of the output signals from the array. The system enables the fast synchronous detection of the ac signals from the array, this operation being performed within a Labview program.

This solution is also very cost effective, because parallel processing of the signals would require the use of multiple lock-in amplifiers.

Figure 42 shows different possible configurations of the signal conditioning and data acquisition for an array-based eddy current system. The output signals of sensors can be multiplexed and sequentially processed using a lock-in amplifier - Figure 42a. This solution requires on-board circuitry including multiplexers and control circuits. The main disadvantage of this solution is the low speed. If the lock-in amplifier's time constant is t_c and the number of sensor of the array is N, the time needed to process all outputs is N t_c. Figure 42b shows a configuration using N lock-in amplifiers to process the output signals in parallel. This solution is faster, the time needed to process all signals being t_c. However, the cost of N lock-in amplifiers is significant, making this solution inadequate, especially for large arrays.

The solution developed by Albany Instruments uses software signal processing that enables the parallel processing and thus eliminating the cost of external lock-in amplifiers – Figure 42c. The output signals of the sensor array are connected directly to the inputs of a data acquisition card. The data acquisition card contains instrumentation amplifiers for each channel. The amplified signals are subsequently demodulated using a reference sinusoidal signal provided by the computer to the excitation coil of the eddy current system. The synchronous demodulation for each channel is performed within a Labview program developed by Albany.

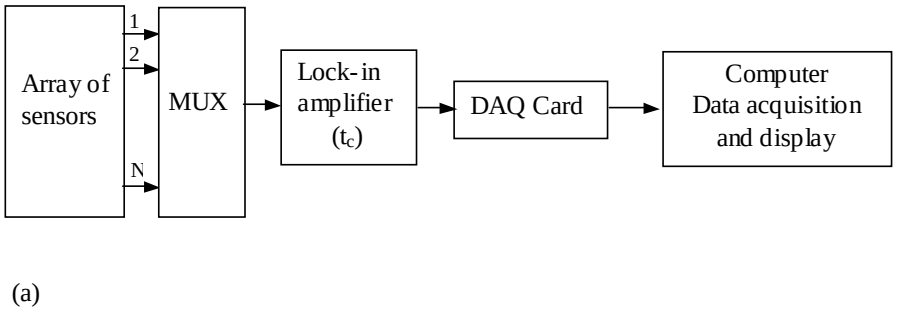

(a)

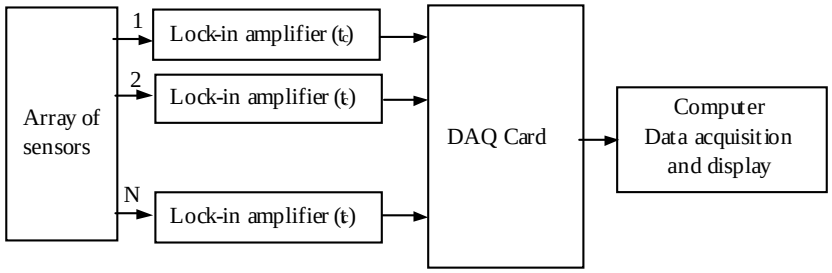

(b)

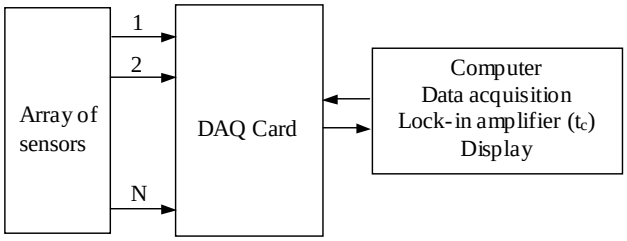

(c)

Figure 42. Configurations of signal processing and data acquisition for (a) GMR array in eddy current applications: a. using multiplexing; (b) parallel processing using multiple lock-in amplifiers; (c) parallel processing using embedded lock-in amplifiers within software programs.

The new data acquisition system was tested to map the AC magnetic field created by a small coil using a high-resolution linear GMR array provided by NVE. The senor array comprises 16 elements in half-bridge configuration spaced at 15 μm. The total length spanned by the array is 225 μm. In order to create a magnetic field gradient within this small distance, a thin solenoid coil was manufactured. The coil has a diameter of 0.6 mm diameter and a length of 3 mm and contains 30 turns of 0.1 mm diameter copper wire. A ferromagnetic core was used to enhance the field at the sensor array location. The array was positioned such that it measures the magnetic field in the direction of the solenoid axis. The radial distribution of this component of the magnetic field has a maximum on the solenoid axis. The coil was scanned above the sensor array using a coordinate measuring machine. The gap between the tip of the coil and the sensor array board was about 0.1 mm.

A sinusoidal current of 0.8 A amplitude and 100 Hz frequency was passed through the coil. This sinusoidal signal was provided from the computer via a current amplifier. The same signal provided the reference signal for the synchronous demodulators embedded within the data acquisition program. A MIO16XE data acquisition card having 16 analog inputs and two analog outputs was used in this experiment. Only 8 output signals – spaced at 30 μm - of the array were monitored (1, 3, 5,…, 15). This selection is because, in a previous measurement, we observed that sensor 6 in the array has a significantly lower sensitivity than the rest of the sensors. The outputs of the sensors were directly connected to the analog inputs of the DAQ card. The supply voltage for the array of half-bridges was 1.5 V. In order to eliminate the need of high-pass filter to suppress the DC output voltage of each sensor, a dual power source was used to provide +0.75 V and –0.75 V to the half-bridges. The amplification of the DAQ card instrumentation amplifiers was set at 50.

The coil was scanned above the sensor array at a speed of 0.1 mm/s. Figure 43 shows the 3-D map of the magnetic field magnitude measured by the eight sensors of the array as a result of this scan. It can be noticed that sensor #6 (of the eight sensors) was scanned across the solenoid axis (maximum magnitude of the magnetic field).

This experiment demonstrates the ability of the new data acquisition system to monitor the output signals of an array of GMR sensors in real time. The system has the advantage of parallel processing (high-speed) using software signal processing instead of external lock-in amplifiers (low cost).

Additional results using this data acquisition system are contained in the section on reports of results during the extension period.

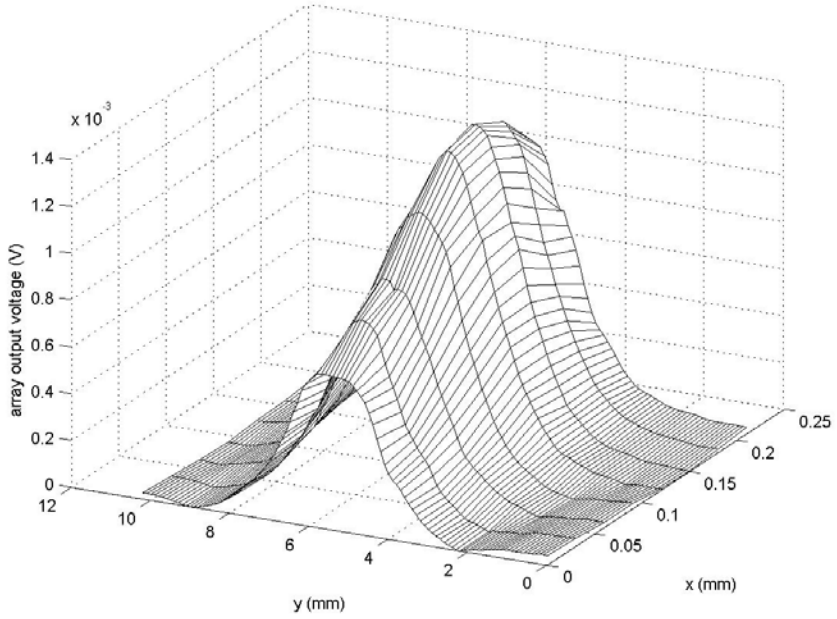

Figure 43. Magnitude map of the sensor array outputs when the coil was scanned above the GMR sensor array.

7. Test On Specimens Provided by the US Air Force

During this program, Albany Instruments, Inc. tested specimens provided by the program monitor. The eddy current probes and methods previously developed under this project have been used to detect the second-layer cracks around fasteners disposed in a row. Two cracks were detected in two of these specimens. The location of one crack was known – indicated by the program monitor.

Sample geometry

Five samples, containing second-layer cracks around fastener holes, have been provided for testing. The samples have identical geometry, which is schematically shown in Figure 44. Each sample consists of a structure of two rectangular aluminum plates held together by ten Taper lock fasteners. First aluminum layer has a thickness of about 7 mm (0.275'), the second layer being 4.3 mm (0.17') thick. The diameter of holes is 6.3 mm (0.25') in depth, and 9.5 mm (0.375') at the surface to fit the buried-head fasteners. The distance between fasteners is about 19 mm (0.75') and the width of the plates is about 50 mm (1.95'). The samples are covered with a thin layer of protective paint. An

unspecified number of cracks are located around the fastener holes in the second layer.

The program monitor has specified the location of the cracks only in one specimen (B4-21). This specimen contains a left-side crack at hole # 2 and a right-side crack at hole # 8. Four of the five specimens contain one ferromagnetic fastener that can be easily detected.

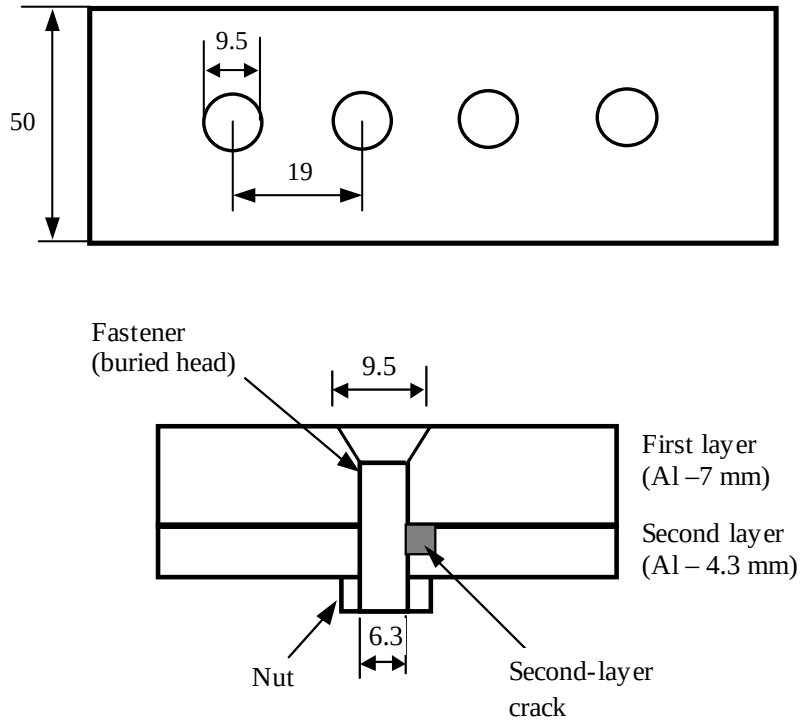

Figure 44. Schematic diagram showing AF samples geometry. Dimensions are given in mm.

Probe configuration

The geometry of the probe and the scanning of the specimens are shown in Figure 45. The probe consists of an excitation coil having a rectangular cross-section and a GMR sensor located on one symmetry axis of the rectangular cross-section. The sensitive axis of the GMR sensor is perpendicular to the symmetry axis of the coil, within the plane of the cross-section. The probe is scanned along the symmetry axis of the specimen (of the fastener row). During scanning the symmetry axis of the coil coincides with the symmetry axis of the fastener row. When the probe is scanned along the longitudinal axis of the specimen, due to the symmetry of the magnetic field at the sensor location, the

probe's output is theoretically zero. A crack on one side of a hole breaks the symmetry of the field, producing a non-zero sensor output.

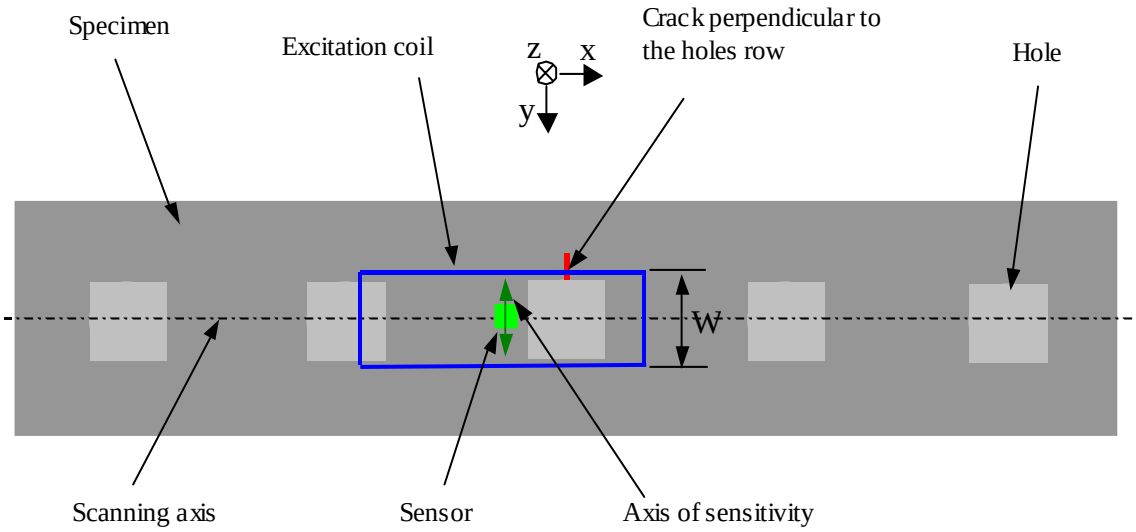

Figure 45: Schematic diagram of an eddy current probe based on a rectangular excitation coil and a GMR sensor. The probe is scanned along the axis of the fasteners row. The sensitive axis of the sensor is perpendicular to the scanning axis

For the measurements performed on the Air Force Research Lab specimens, a rectangular excitation coil of 10 mm width (W) - approximately equal to the diameter of the fastener head – has been manufactured. The coil has a length of 20 mm and contains 18 turns.

The position of the GMR sensor (high-temperature multi-layer) can be adjusted to align it with respect to the coil. The probe was scanned above the specimen using a coordinate measuring machine. During the tests the frequency and the phase of the excitation current were adjusted to obtain the maximum sensitivity of the probe to the second-layer cracks. A current of about 1 A amplitude has been passed through the excitation coil. The signal from the sensor was amplified (x20) using a standard low-noise preamplifier (SR560). The in-phase (X) and out-of phase (Y) amplitudes were extracted using a SR 850 lock-in amplifier.

Experimental results

Measurements were performed on two specimens: B4-21 and B4-22. The sample B4-21 has two cracks (at holes #2 – left crack and #8 – right crack). It

also contains a ferromagnetic fastener at hole #5. The ferromagnetic fastener strongly influences the output of the GMR sensor when the probe approaches this fastener. It was observed that the influence of the ferrous fastener started when the GMR sensor was located above the center of the adjacent fastener. Therefore the data was recorded when the probe was scanned from hole #10 to hole #6. Another scan was performed from hole #4 to hole #1 using the same alignment of the probe and specimen.

First, the frequency was varied to maximize the crack signal. The optimum frequency was obtained at 400 Hz. All results shown in this report were taken at this frequency. The phase was also adjusted to separate the cracks signal from the background signal caused by the holes edge and fasteners. The optimum phase of the reference signal was about -45 degrees. At this phase the crack signals can be observed on the Y-output of the lock-in, while the background signal can be identified on the X-output.

The results from scanning from hole # 10 to hole #6 of the specimen B4-21 are shown in Figure 46. The out-of-phase (Y-output) signal of the lock-in amplifier has a clear positive peak that corresponds to the right-side crack located at the hole #8. There is also a negative peak that corresponds to the hole #10. This peak was obtained because hole #10 is the ending hole of the row (does not have adjacent hole on each side). Improving the probe-specimen alignment can reduce this peak. The in-phase (X-output) of the lock-in amplifier shows the signal produced by holes edges and fasteners, signal that is due to misalignments of the probe elements (coil-sensor) and between probe and specimen. The location of the holes can be determined from this plot. The minima of the signal correspond to the position of the GMR sensor above the center of each hole. The first minimum corresponds to the hole #10, the last minimum to the hole #6. The sharp decrease of the signal (on both plot) following the hole #6 is due to the influence of the ferromagnetic fastener (located in hole #5).

The second scan between holes #4 and #1 on specimen B4-21 did not result in a clear crack signal from hole #2. The proximity of this hole to ending hole #1 makes the detection more difficult. The detection of this crack requires further improvement of the alignment of the experimental system.

The results scanning from hole # 1 to hole #5 of the specimen B4-22 are shown in Figure 46. The out-of-phase (Y-output) signal of the lock-in amplifier has a negative peak located at the hole #4. This leads to the conclusion that there is a left-side crack at the hole #4 in the second layer of this specimen. The frequency at which this signal was recorded was 400 Hz (the same as for B4-21) and the phase of the reference signal of the lock-in amplifier was -50 deg. As in the case of the other specimen, the end hole #1 produces a negative peak. The X-output can be used as a reference to determine the location of the holes. The first

minimum corresponds to hole #1, the last minimum to the hole #5. The sharp decrease in the signal following the hole #5 is due to the ferromagnetic fastener that is located in hole #6.

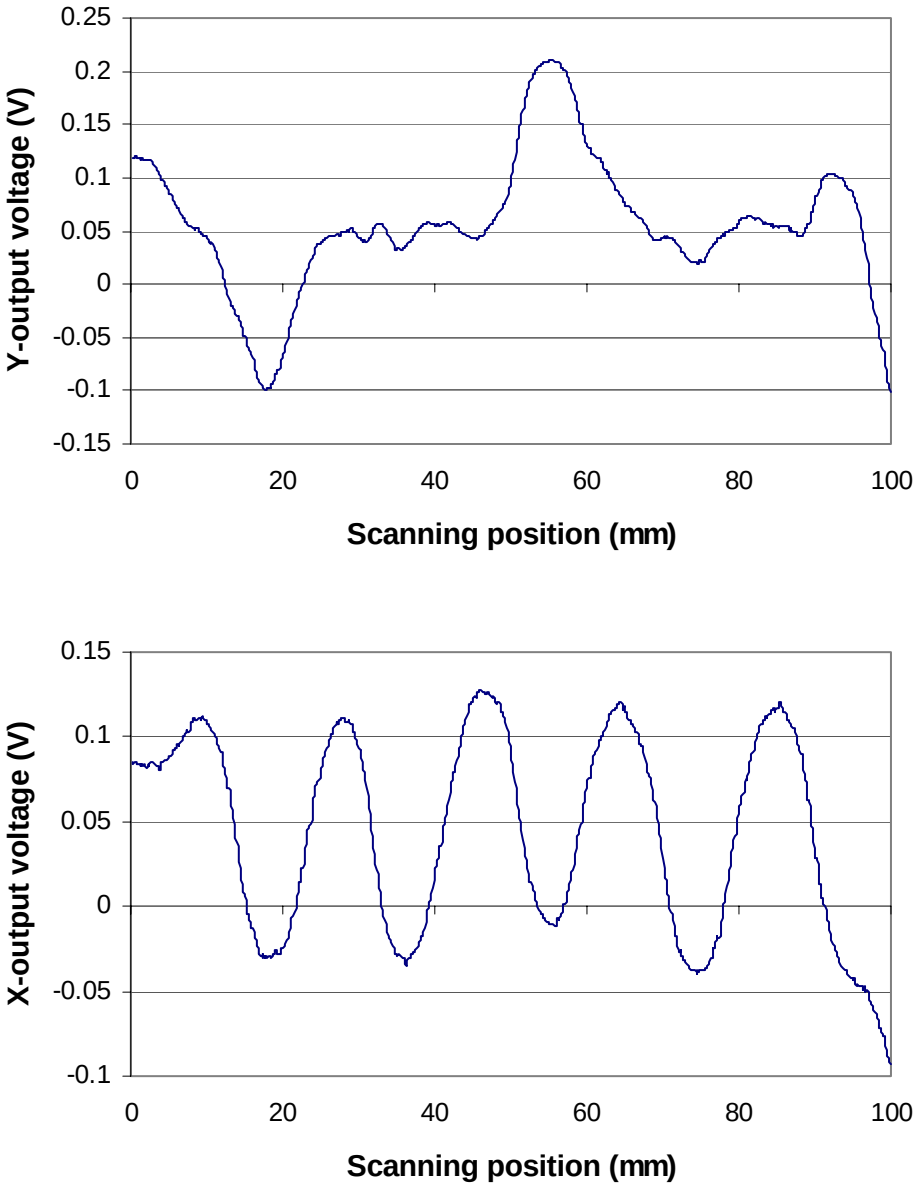

Figure 46. Out-of-phase (top) and in-phase (bottom) output signals from the probe when scanned along the specimen B4-21, from hole #10 to hole #6. The first minimum in the X-output signal corresponds to the position of the probe above the center of hole #10. The largest positive peak on Y-output signal indicates the presence of a right-side crack at hole #8.

COMMERCIALIZATION ACTIVITIES

Under a Non Recurring Engineering (NRE) project funded by a major credit card manufacturer NVE developed proof-of-concept sensor arrays for a security improvement system for credit cards. Initial results were demonstrated using the 15 μm spacing 16-element half-bridge GMR sensor arrays. The sensors can accurately detect the position of the edge of the magnetic stripe, the flux transitions, and the magnetic media noise. These sensors are similar to the array sensors used in tests in this report except for the presence of small plated flux return elements. The flux return elements limit the area that the sensors see and improve their performance as half bridges measuring the z component of the flux. We have quoted a second wafer run of GMR sensor arrays with modifications to improve sensitivity and resolution to the company we have been working with that is developing a proprietary system to image magnetic media for security purposes. Initial results on the first batch of 16-element sensor arrays with flux guides and flux returns are promising. We have ideas on methods of improving sensitivity and resolution. If this batch of sensor arrays has the required characteristics, the next step will be 100-sensor arrays on semiconductor underlayers to handle amplification and multiplexing.

We supplied some 16-element, half-bridge sensor array chips mounted and die bonded on circuit boards to TPL in Albuquerque, NM in support of an SBIR they are working on concerning linear position sensing.

Follow-up contacts with Pure Technologies, which were a result of presentations at Sensors EXPO, resulted in a purchase order for SDT sensors for inspection of cables in suspension bridges and other structural health monitoring systems

Meet with Glen Light of Southwest Research Institute at the Aeromat Conference in June 2002. NVE now has provided a quote to SwRI in support of a proposal submitted to Wright Patterson Air Force Base on developing GMR sensor arrays for eddy-current sensing of defects in engine components.

We provided Ray Rempt of Boeing Corporation in Seattle with ROM time and pricing estimates for developing GMR and SDT sensor arrays for NDE programs. These estimates included both sensor arrays of either GMR or SDT and integrated sensor arrays with semiconductor underlayers.

A discussion was held with Lion Precision with respect to possible eddy current work using GMR/SDT sensors through their newly formed division, Lion Precision Inductive in Colorado Springs, Colorado.

Albany Instruments subcontracted with ZTS (a consultant) for several summary reports on the eddy-current probe industry. These reports are mentioned by title and referenced by the monthly report in which they appeared.

SUMMARY REPORT ON MATERIALS FOR PROBE MANUFACTURE – Sixth Monthly Report

ANNUAL EDDY CURRENT MARKET ASSESSMENT (US/WORLDWIDE) – Ninth Monthly Report

SUMMARY REPORT ON MACHINABLE CERAMICS AND CONNECTORS FOR EDDY CURRENT PROBES – Tenth Monthly Report

MAJOR EDDY CURRENT EQUIPMENT MANUFACTURERS UNIQUE FEATURES, MODE OF OPERATION, PRICING, ETC – Fifteenth Monthly Report

SUMMARY REPORT ON EDDY CURRENT PROBE MANUFACTURERS – Sixteenth Monthly Report

PATENT APPLICATIONS AND DISCLOSURES

Substantial intellectual property was developed by Albany Instruments/University of North Carolina-Charlotte. A total of three disclosures have been written and an utility patent has been filed on one of them.

1. Invention Report No. AI-IR-2002-003

Date: June 25, 2002
Title of the invention: **Eddy current probes and methods for detecting buried cracks around fastener holes**
Inventor: Teodor Dogaru
Employer: Albany Instruments Inc.

This invention details new eddy current probes and methods for detecting cracks around fastener holes as described in the following Albany's progress reports submitted to NVE for the AF00-145 project: April-May 2002 (12^{th} monthly), May-June 2002 (13^{th} monthly), June-July 2002 (14^{th} monthly).

The invention includes the eddy current probes based on flat, linear or rectangular excitation coils and magnetic sensors having the sensitive axis in the plane of the specimen under test. Eddy current probes based on arrays of sensors and gradiometer sensors are also included in this invention. Probe configurations based on a single excitation coil, double-coil and three-coils are described in this invention report.

2. Invention report No. AI-IR-2002-006

Date: November 1, 2002
Title of the Invention**: Eddy current probe based on an array of magnetoresistive sensors**
Inventor: Teodor Dogaru
Employer: Albany Instruments Inc.

This invention details the eddy current probe described in the following Albany's progress reports submitted to NVE for the AF00-145 project: February-March 2003 (22nd monthly).

The probe comprises a flat rectangular coil and a linear array of magnetoresistive sensors (as shown in Figure 1 of the above mentioned report).
A provisional application has been filed with USPTO for this disclosure:
Application No.: 60/424,874
Filing date: 11/12/2002

3. Utility patent application filed – Attorney Docket No. 46872/276853

Filing date: July 11, 2003
Title of the utility patent application: **Probes and methods for detecting defects in metallic structures**
Inventor: Teodor Dogaru
Employer: Albany Instruments Inc.
Application Number: Not yet assigned
This patent application includes the probes and methods described in the two disclosures above. It also includes the portable eddy current system as described in the following Albany's progress reports submitted to NVE for the AF00-145 project: July-August 2002 (15), August-September 2002 (16), September-October 2002 (17), March-April 2003 (23).

This system features software simulated lock-in amplifiers to replace standard lock-in commonly used in eddy current system. This system can be used for single sensor or sensor array-based eddy current probes. For the array-based eddy current systems, multiple software lock-in amplifiers are used for parallel processing of the sensors signals

PRESENTATIONS AND PUBLICATIONS

The following presentations and publications included some of the results from this program.

Presentations

1. Carl Smith, Bob Schneider, Stuart T. Smith, and Teodor Dogaru, “Non-Destructive Test (NDT) Utilizing Spin-Dependent Tunneling Sensors,” MAT2001 International Conf. Material Testing and Research, Nuremberg, Germany, May 10, 2001.
2. Mark Tondra, Carl Smith Dexin Wang, and S. Smith, “Magnetoresistive Sensors for Industrial Applications: Eddy Current Nondestructive Evaluation and Position Sensing,” Twentieth Annual conference on Properties and Applications of Magnetic Materials, Chicago, IL, May 15, 2000.
3. Carl Smith, Bob Schneider, Stuart T. Smith, and Teodor Dogaru, “SDT Magnetic Sensors for Non-Destructive Test and Other Low-Field Applications,” 75 minute tutorial at Sensors Expo, Chicago, IL, June 6, 2001.
4. Carl Smith, Bob Schneider, Stuart T. Smith, and Teodor Dogaru, “SDT Magnetic Sensors for Non-Destructive Test and Other Low-Field Applications,” 75 minute tutorial at Sensors Expo, Philadelphia, PA, October 3, 2001.
5. Carl Smith, and Bob Schneider, “Chip-Size Magnetic Sensor Arrays,” 75 minute tutorial at Sensors Expo, San Jose, CA, May 21, 2002.
6. C. H. Smith, R. W. Schneider, T. Dogaru, and S. T. Smith, “Chip-Size Magnetic Sensor Arrays for Eddy-Current Testing,” AeroMat 2002 Conference, Orlando, FL, June 11, 2002.
7. T. Dogaru, S. T. Smith, C. H. Smith, and R. W. Schneider, “Eddy Current Detection of Deeply Buried Cracks Around Fastener Holes: Experimental Study,” AeroMat 2002 Conference, Orlando, FL, June 11, 2002.
8. C. H. Smith, R. W. Schneider, T. Dogaru, and S. T. Smith, “GMR Magnetic Sensor Arrays for NDE Eddy-Current Testing,” Quantitative Nondestructive Evaluation Conference, Bellingham, WA, July 18, 2002.
9. Carl Smith, and Bob Schneider, “Chip-Size Magnetic Sensor Arrays,” 75 minute tutorial at Sensors Expo, Boston, MA, September 25, 2002.
10. C. H. Smith, R. W. Schneider, and A. V. Pohm, “High-Resolution GMR On-Chip Arrays for Magnetic Imaging,” 47th Annual Conference on Magnetism & Magnetic Materials, Tampa, FL, November 12, 2002.
11. Carl H. Smith, and Robert W. Schneider, “Very Dense Magnetic Arrays for Precision Measurement and Detection,” 75 minute tutorial at Sensors Expo, Chicago, IL, June 4, 2003.
12. C. H. Smith, R. W. Schneider, T. Dogaru, and S. T. Smith, “NDE Eddy-Current Testing with GMR Magnetic Sensor Arrays,” Quantitative Nondestructive Evaluation Conference, Green Bay, WI, July 28, 2003.
13. T. Dogaru, C. H. Smith, W. Schneider, and S. T. Smith, “Deep Crack Detection around Fastener Holes in Airplane Multi-Layered structures Using GMR-based

Eddy-Current Probes," Quantitative Nondestructive Evaluation Conference, Green Bay, WI, July 28, 2003.

Publications

1. Carl Smith, Bob Schneider, Stuart. T. Smith, and Teodor Dogaru, "Non-Destructive Test (NDT) Utilizing Spin-Dependent Tunneling Sensors," *Proceedings of MAT 2001*, (AMA Service GmbH, Wunstof, Germany, 2001), pp. 205-210.
2. Carl Smith, Bob Schneider, Stuart. T. Smith, and Teodor Dogaru, "SDT Magnetic Sensors for Non-Destructive Test and Other Low-Field Applications," *Proceedings of Sensors Expo and Conference Spring 2001,* (Advanstar Publications, Peterborough, NH, 2001), pp 417-427.
3. Teodor Dogaru, Carl Smith, Bob Schneider, and Stuart. T. Smith, "New Directions in Eddy Current Sensing," *Sensors Magazine*, vol. 18, no. 6, (June 2001)*,* pp. 56-62.
4. Carl Smith, Bob Schneider, Stuart. T. Smith, and Teodor Dogaru, "SDT Magnetic Sensors for Non-Destructive Test and Other Low-Field Applications," *Proceedings of Sensors Expo and Conference Fall 2001,* (Advanstar Publications, Peterborough, NH, 2001), pp 53-63.
5. Carl Smith, and Bob Schneider, "Chip-Size Magnetic Sensor Arrays," *Proceedings of Sensors Expo and Conference Spring 2002,* (Advanstar Publications, Peterborough, NH, 2002), pp 95-104.
6. C. H. Smith, R. W. Schneider, T. Dogaru, and S. T. Smith, "GMR Magnetic Sensor Arrays for NDE Eddy-Current Testing," *Review of Progress in Quantitative Nondestructive Evaluation*, *Vol. 22*, ed. by D. O. Thompson and D. E. Chimenti, (American Institute of Physics, Melville, NY, 2003) pp 419-426.
7. Carl Smith, and Bob Schneider, "Chip-Size Magnetic Sensor Arrays," *Proceedings of Sensors Expo and Conference Fall 2002, Boston,* (Advanstar Publications, Peterborough, NH, 2002), pp 287-296.
8. Carl Smith, Bob Schneider, and Arthur Pohm "High-Resolution, Chip-Size Magnetic Sensor Arrays," *Sensors Magazine*, vol. 20, no. 3, (March 2003)*,* pp. 44-49.
9. C. H. Smith, R. W. Schneider, and A. V. Pohm, "High-resolution giant magnetoresisance on-chip arrays for magnetic imaging*," J. Appl. Phys*., vol. 93, no. 10, (2003), pp. 6864-6866.
10. Carl H. Smith, and Robert W. Schneider, "Very Dense Magnetic Arrays for Precision Measurement and Detection," *Spring 2003 Proceedings of Sensors Expo & Conference (on CD),* (Advanstar Publications, Peterborough, NH, 2003), 10 pages.

11. C. H. Smith, R. W. Schneider, T. Dogaru, and S. T. Smith, “NDE Eddy-Current Testing with GMR Magnetic Sensor Arrays,” to be published in *Review of Progress in Quantitative Nondestructive Evaluation*, *Vol. 23*, 8 pages.
12. T. Dogaru, C. H. Smith, W. Schneider, and S. T. Smith, “Deep Crack Detection around Fastener Holes in Airplane Multi-Layered structures Using GMR-based Eddy-Current Probes,” to be published in *Review of Progress in Quantitative Nondestructive Evaluation*, *Vol. 23*, 8 pages.

REPORT PREPARER:

Carl H. Smith, PI
(973) 635-7576